Korea-Australia Rheology Journal
Vol. 22, No. 4, December 2010 pp. 0-0

Shear-banding instabilities

Jan K.G. Dhont[1], Kyongok Kang[1], M.P. Lettinga[1] and W. J. Briels[1]
[1]*Forschungszentrum Jülich, IFF/ Weiche Materie, D-52425 Jülich, Germany*
[2]*University of Twente, Computational Biophysics, Postbus 217, 7500 AE Enschede, The Netherlands*
(Received A 00, 2010; final revision received A 00, 2010; accepted A 00, 2010)

Abstract

Gradient-banding and vorticity-banding instabilities, as well as a shear-induced instability due to shear-gradient induced mass transport will be discussed. Various scenarios that underly these instabilities are addressed and simple constitutive relations that allow for a (semi-) quantitative analysis are proposed. A relatively simple constitutive equation that has been proposed some time ago is reviewed, which captures a number of the experimentally observed gradient-banding phenomena. This constitutive equation is based on the usual formal expansion of the stress tensor with respect to gradients in the flow velocity, but now including the second order term. The second order term is necessary to describe the relatively large spatial gradients within the interface between the two bands. The resulting simple constitutive equation is shown to give rise to stationary gradient-banded states, where the shear rates within the bands are constant, it describes stress selection under controlled rate conditions and explains why banding can not occur under controlled stress conditions. The simple constitutive equation does not include coupling to concentration, which may give rise to banding also under controlled stress conditions. Two examples of mechanisms that lead to the strong shear thinning that is necessary for gradient banding are discussed: (i) transient forces due to entanglements in polymer systems, and (ii) critical slowing down. The latter mechanism is shown to be important for a worm-like micellar system. The mechanism that leads to vorticity banding is still under debate. Vorticity banding of fd-virus suspensions within the two-phase isotropic-nematic coexistence will be discussed. Experiments on the kinetics of banding and particle-tracking experiments lead to a recently proposed mechanism for the vorticity-banding instability, where the instability is identified as an elastic instability similar to the polymer-Weissenberg effect. The role of polymer chains in the classic Weissenberg effect is now played by inhomogeneities formed during the initial stages of phase separation. For other systems than fd-virus suspensions that exhibit vorticity banding, the inhomogeneities general have a different origin, like in weakly aggregated colloids and worm-like micellar systems where the inhomogeneities are the colloidal aggregates and the worms, respectively. An instability that has been discovered some time ago, which is an instability due to shear-gradient induced mass transport is also discussed. The coupling between shear-gradients and mass transport has been formally introduced through a shear-rate dependent chemical potential, of which the microscopic origin was not explained. It will be shown that the microscopic origin of this coupling is related to the shear-induced distortion of the pair-correlation function. Contrary to the stationary gradient-banded and vorticity-banded state, it is not yet known what the stationary state is when this shear-concentration-coupling instability occurs.

Keywords :

1. Introduction

The two main types of banding instabilities are gradient banding and vorticity banding. In case of gradient banding in a Couette cell, the stationary state is one where two bands coexist, which extend in the gradient direction. The left sketch in Fig. 1 gives a top view of such a banded state in a Couette geometry. The shear rate within each of the two bands is essentially spatially constant, and the two bands are connected by a sharp interface where there is a very strong spatial variation of the shear rate. In case of vorticity banding, regular bands are formed which are stacked in the vorticity direction, as sketched on the right in Fig. 1. The bands are visible, for example, because the two types of bands have a different turbidity or because they are both birefringent but with somewhat different orientation of the optical axes. A third kind of instability has

*Corresponding author:

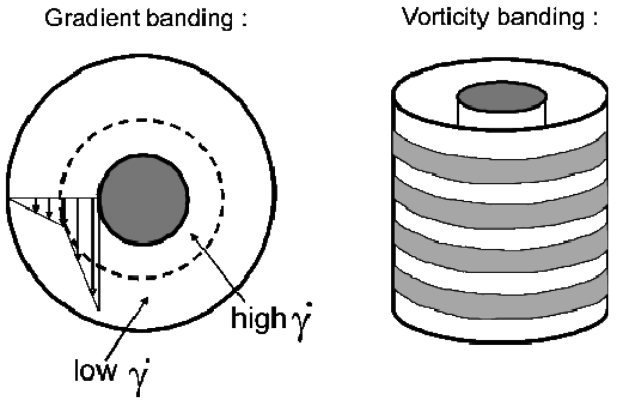

Fig. 1. Sketches of the stationary states in a Couette cell in case of gradient banding (left figure, top view) and vorticity banding (right figure, side view).

been described for the first time by Schmitt in Ref.(Schmitt *et al.*, 1995). This is an instability that is due to mass transport that is induced by spatial gradients in the shear rate. Probably because the origin of such a coupling is unclear, this instability has largely been ignored. We will refer to this instability as the "shear-concentration-coupling instability", or in abbreviation the SCC-instability.

This paper consists of three main sections, one on gradient banding (including two sections on entanglement forces and banding in a worm-like micellar system), one on vorticity banding, and one on the SCC-instability. A minimal model that describes many features of gradient banding is discussed in section 2. An important mechanism in many polymer systems that is at the origin of severe shear thinning, a necessary requirement for gradient banding, is related to transient forces resulting from entanglements. These forces are briefly described in section 3. Experiments are presented on a worm-like micellar system in section 4 that indicate that the strong shear thinning in this system is due to critical slowing down of orientational diffusion due to the vicinity of the isotropic-nematic spinodal. Vorticity banding is discussed in section 5, where experiments on suspensions of colloidal rods are described that lead to the proposition that this is an elastic instability, similar to the Weissenberg effect for polymers. In section 6 the SCC-instability is discussed, where the microscopic origin of the mass flux induced by gradients in the shear rate is shown to be related to the shear-induced distortion of the pair-correlation function.

Recent review papers that address banding phenomena include Ref.(Olmsted, 1999) which contains a comprehensive overview of existing literature, Ref.(Vermant, 2003) where shear-induced bundles and strings as well as near-critical and weakly aggregated colloids are discussed, and Refs.(Cates *et al.*, 2006; Berret, 2005) which extensively discuss the rheology and banding of micellar systems. Reference (Cates *et al.*, 2006) also contains a section on time-dependent phenomena. A recent treatment of time-dependent phenomena can be found in Ref. (Fielding, 2007). A collection of four overview papers on shear banding have recently been published in Rheologica Acta (Callaghan, 2008; Dhont *et al.*, 2008; Olmsted, 2008; Manneville, 2008).

2. Gradient banding

Here we will present a simple model (Dhont, 1999; Olmsted, 1999; Lu *et al.*, 2000) that explains a number features that are seen experimentally. Consider a laminar flow in a two-plate geometry in the x-direction, and with y the gradient direction. Neglecting variations of the flow velocity u in the x- and z-directions, the Navier-Stokes equation takes the form,

$$\rho_m \frac{\partial u(y,t)}{\partial t} = \frac{\partial \Sigma(y,t)}{\partial y}, \qquad (1)$$

where ρ_m is the overall mass density of the suspension and $\sum$ is the shear stress. The standard expression for the stress is $\dot{\gamma}\eta$, with $\dot{\gamma}$ the local shear rate and η the shear viscosity. This text-book expression for the shear stress is obtained from a formal expansion up to leading order in velocity gradients. This standard shear stress will be

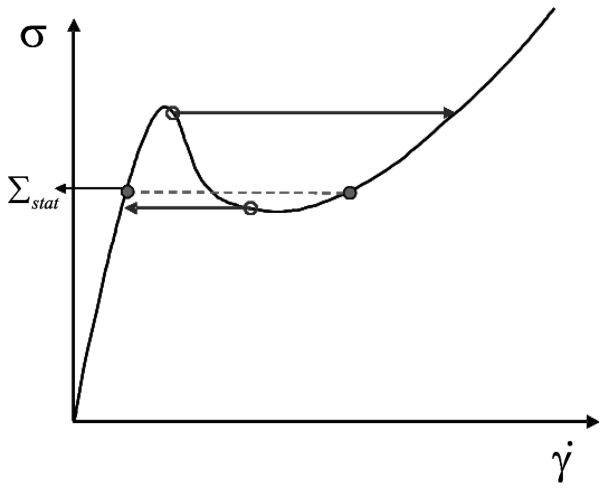

Fig. 2. The "van der Waals loop-like" form of the standard shear stress $\sigma = \dot{\gamma}\eta$ as a function of the shear rate, which is the stress of the homogeneously sheared system, before banding occurs. The dashed, red horizontal line marks the selected stress in the stationary state under controlled shear-rate conditions, according to the "modified" equal-area Maxwell construction (7). The horizontal arrows in blue correspond to bottom- and top-jumps that are observed under controlled stress conditions in case the imposed stress is not equal to the modified-equal-area stress.

denoted by $\sigma = \dot{\gamma}\eta$, and is the stress of a system in which spatial gradients of the shear rate are not too large.

A stationary gradient-banded state exhibits usually two regions (the "bands") where the shear rate is independent of position, which regions are separated by an "interface" in which spatial gradients in the shear rate are very large (see the left sketch in Fig. 1). Within the interface, the standard stress is not sufficient to capture the large spatial gradients, and the above mentioned spatial-gradient expansion of the stress tensor must be extended to the next higher order term. From symmetry considerations it is readily seen that this expansion reads (Dhont, 1999),

$$\Sigma(y,t) = \eta(\dot{\gamma}(y,t))\dot{\gamma}(y,t) - \kappa(\dot{\gamma}(y,t))\frac{\partial^2 \dot{\gamma}(y,t)}{\partial y^2}. \quad (2)$$

The proportionality constant κ of the second order derivative of the shear rate is referred to as the *shear-curvature viscosity* (Dhont, 1999). As will be seen, the second order contribution prevents the very fast development of unphysically large gradients in the flow velocity, and is a necessary ingredient to describe the stationary banded state. An alternative approach that achieves these features is to include a diffusive term in equations of motion for the stress tensor, where the corresponding diffusion coefficient is referred to as the *stress diffusion coefficient* (Lu *et al.*, 2000; Spenley *et al.*, 1996; Radulescu *et al.*, 2003; Yuan *et al.*, 1999; El-Kareh *et al.*, 1989). There seems to be no simple connection between the shear-curvature viscosity and the stress-diffusion coefficient.

Experiments indicate that for systems which exhibit gradient banding, the standard stress exhibits a van der Waals loop-like behaviour as depicted in Fig. 2. This is the stress that is measured for the homogeneously sheared system, before banding occurs. According to eq. (1), the stress is constant throughout the gap of the two-plate geometry for a stationary state. This implies that for a stationary gradient banded state, the stress in the two bands are equal (as indicated by the two red points in Fig. 2). In going through the interface, however, the van der Waals loop is probed, which violates the requirement that the stress must be constant. The standard stress is therefore not sufficient to describe gradient banding. The second order term in eq. (2) is necessary to render the total stress spatially constant, also within the interface.

Assuming a banded velocity profile, it is easily verified (Dhont, 1999) that a y-independent stress, also within the interface, is only possible if,

$$\kappa > 0. \quad (3)$$

Furthermore, the shear-curvature viscosity is expected to vanish in a shear-rate range where the viscosity attains its high shear-rate value,

$$\lim_{\dot{\gamma}\to\infty} \kappa(\dot{\gamma}) = 0. \quad (4)$$

The question may be asked which value for the stationary stress $\sum_{stat}$ in Fig.2 is actually selected. Any value of $\sum_{stat}$ in Fig. 2 satisfies the requirement that the stresses in the two bands are equal, but there is a unique value that also renders the total stress within the interface equal to that within the bands. The stress selection rule that sets the stress in the stationary banded state can be derived from the constitutive equation (2). Suppose that a stationary banded structure exists (as depicted in Fig.1, left figure). From eq.(2),

$$\Sigma_{stat} = \eta(\dot{\gamma}(y))\dot{\gamma}(y) - \kappa(\dot{\gamma}(y))\frac{d^2\dot{\gamma}(y)}{dy^2}. \quad (5)$$

Since within the two bands the shear rate is spatially constant, we have,

$$\int_{\dot{\gamma}_-}^{\dot{\gamma}_+} d\dot{\gamma}\, \frac{d^2\dot{\gamma}(y)}{dy^2} = \frac{1}{2}\int_{y_-}^{y_+} dy\, \frac{d}{dy}\left(\frac{d\dot{\gamma}(y)}{dy}\right)^2 = 0, \quad (6)$$

provided that the shear rate is a monotonic function of position. Here, $\dot{\gamma}_+$ and $\dot{\gamma}_-$ are the shear rates in the high shear-rate and low shear-rate band, respectively, while y_+ and y_- are positions within the two corresponding bands. Integration of eq. (5) thus leads to,

$$\int_{\dot{\gamma}_-}^{\dot{\gamma}_+} d\dot{\gamma}\, \frac{\eta(\dot{\gamma})\dot{\gamma} - \Sigma_{stat}}{\kappa(\dot{\gamma})} = 0, \quad (7)$$

This is the *stress-selection rule* within the present minimal model (Dhont, 1999; Olmsted, 1999; Lu *et al.*, 2000). The system will select a stress $\sum_{stat}$ in the stationary state such that it satisfies eq.(7). For a shear-rate independent shear-curvature viscosity, this stress-selection rule implies an equal-area Maxwell construction. According to eq. (4), however, the shear-curvature viscosity is shear-rate dependent, which shifts the selected stress to somewhat lower values as compared to the equal-area stress, as depicted in Fig. 2.

The system has the freedom to select its stress when the shear rate is controlled during an experiment. When the stress is controlled, and the applied stress is different from $\sum_{stat}$ as given in eq. (7), shear banding can not occur since in a stationary shear-banded structure the stress must be equal to $\sum_{stat}$. Hence, *shear banding can not occur in a stress-controlled experiment*. There are now two possible scenarios : (i) the flow profile always has a uniform shear rate. In this case, the stress jumps from its maximum to the stable branch at higher shear rate (and similarly for decreasing stress), or (ii) a flow profile exists which is neither a banded state nor a state where the shear rate is homogeneous, but rather a flow profile where the shear rate varies throughout the entire gap of the cell. "*Bottom- and top-jumps*" under controlled stress conditions, are observed in, for example, micellar systems (Yesilata *et al.*, 2006; Cappelaere *et al.*, 1997), in a colloidal crystalline system (Chen *et al.*, 1992), in supra-molecular polymer solutions (van der Gucht *et al.*, 2006) and in dispersions of

clay particles (ten Brinke *et al.*, 2007). The jumps are indicated in Fig. 2 by the horizontal arrows.

There are experiments where banding is also observed under controlled stress conditions. This is due to a strong coupling of stress to concentration, which is neglected in the present minimal model. The variation of concentration is now an additional degree of freedom that facilitates banding also under controlled stress conditions. Banding of systems consisting of rod-like particles, including both coupling to concentration and orientational order, is discussed in Refs. (Olmsted *et al.*, 1999; 1997). Since the concentrations within the bands adjust to the applied shear rate, the shear rates within the bands are now depending on the applied shear rate. This renders the stationary stress $\sum_{stat}$ in the banded state dependent on the applied shear rate (Olmsted *et al.*, 1999; Olmsted, 1999), and explains the sometimes observed "tilted stress plateau" (Cappelaere *et al.*, 1997; van der Gucht *et al.*, 2006; Berret *et al.*, 1998; Hu *et al.*, 2005; Lerouge *et al.*, 2006; Lerouge *et al.*, 2000; van den Noort *et al.*, 2007). Coupling to concentration has been discussed, within particulate models, in Refs.(Olmsted, 1999; Olmsted *et al.*, 1999; Fielding, 2003).

To see under which conditions a linear flow profile becomes unstable, a stability analysis of the Navier-Stokes equation (1) can be performed. Let $\dot{\gamma}_0$ denote the applied shear rate. The "natural" flow profile in a two-plate geometry would be one where the velocity u is equal to $\dot{\gamma}_0 y$, where y is the distance from the lower, stationary plate. This linear flow profile is perturbed, that is, $u(y,t) = \dot{\gamma}_0 y + \delta u(y,t)$, where $\delta u(y,t)$ is the small perturbation. Substitution into eqs.(1,2) and linearization with respect to δu, assuming stick-boundary conditions, leads to,

$$\delta u(y,t) = \sum_{n=1}^{\infty} \alpha_n \sin\{k_n y\} \exp\left\{-\Lambda_n k_n^2 t\right\}, \tag{8}$$

where the coefficients α_n are determined by the initial form of the perturbation, the wave vectors $k_n = n\pi/L$ (with L the gap width and $n = 1, 2, \cdots$), and,

$$\Lambda_n = \frac{1}{\rho_m}\left[\frac{d\sigma(\dot{\gamma}_0)}{d\dot{\gamma}_0} + \kappa(\dot{\gamma}_0) k_n^2\right]. \tag{9}$$

Clearly, the linear flow profile is unstable when,

$$\frac{d\sigma(\dot{\gamma}_0)}{d\dot{\gamma}_0} \leq -\kappa(\dot{\gamma}_0) k_n^2, \tag{10}$$

for $n = 1$ (and possibly $n > 1$). In case the right hand-side of eq.(10) is very small, this complies with experimental findings that banding occurs when the slope of the standard stress σ (which is the stress of the homogeneously sheared system) versus the applied shear rate is negative (this is found experimentally for worm-like micelles (Berret *et al.*, 1997; Britton *et al.*, 1999; Fischer *et al.*, 2001; Britton *et al.*, 1999; Salmon *et al.*, 2003), poly-crystalline colloids (Imhof *et al.*, 1994, Hunerbein *et al.*, 1996, Palberg, 1996), micellar cubic crystals (Eiser *et al.*, 2000), and most probably this scenario also applies for semi-dilute polyacrylamide solutions (Callaghan, 2000; Britton, 1997). Note that the shear rates where the linear flow profile becomes unstable are *not* exactly at the maximum and minimum of the van der Waals loop. The slope $d\sigma/d\dot{\gamma}$ should be sufficiently negative, depending on the value of κ, before the linear flow profile becomes unstable.

Numerical integration of the equation of motion (1,2) under controlled shear-rate conditions, where the applied shear rate is fixed, indeed leads to regions (the "bands") where the shear rate is constant (Dhont *et al.*, 2008). The simple constitutive equation (2) thus describes many of the observed phenomena related to gradient banding. There are, of course, a number obvious omissions in the minimal model:

(i) The concentration dependence of the shear stress is neglected. As discussed above, the coupling to concentration can lead to banding also under controlled stress conditions. The SCC-instability that will be discussed in section 6 is an instability where a decreasing standard stress with increasing shear rate is not required, and which is entirely the result of such a coupling to concentration.

(ii) Elastic contributions to the stress are neglected. This is of importance for the description of the kinetics of band-formation when the time scale of interest is smaller than the typical relaxation times of elastic stresses Ref.(Goddard, 2003).

(iii) Flow-induced phase transitions are not accounted for. In some systems, flow can induce new phases, which can lead to banded-like flow.

(iv) The minimal model is a scalar theory that neglects normal stresses. Note, however, that the non-local shear-curvature-viscosity contribution could be included in constitutive models which include normal stresses. In Ref.(Briels, 2011) a semi-microscopic theory is presented that derives the shear-curvature contribution to the stress as well as normal stresses that result from transient entanglement forces in polymer systems.

A numerical value for the shear-curvature viscosity for a micellar system has been determined in Ref.(Masselon, 2008) from stationary velocity profile measurements in micro-channels. The linear extent of the channel is so small, that the higher order gradient contribution to the stress in eq. (2) is important in relatively large regions within the channel. Velocity profiles are accurately described with the constitutive relation (2) with a single, shear-rate independent value of $\kappa = 2.1 \times 10^{-10} Ns$ for the shear-curvature viscosity.

The most studied systems that exhibit gradient banding are worm-like micellar systems (experiments on worm-like micelles can be found in Refs. (Yesilata *et al.*, 2006; Berret *et al.*, 1998; Hu *et al.*, 2005; Berret *et al.*, 1997; Britton *et al.*, 1999; Fischer *et al.*, 2001; Salmon *et al.*, 2003; Herle

et al., 2005; Liberato *et al.*, 2006; Miller *et al.*, 2007; Manneville *et al.*, 2007), and theoretical models for worms concerned with banding in Refs.(Spenley *et al.*, 1993; 1996; Vasquez *et al.*, 2007). In some (diluted and concentrated) worm-like systems wall slip is reported (Mannesville *et al.*, 2007; Salmon *et al.*, 2003; Lettinga *et al.*, 2009). Gradient banding is also reported to occur in entangled polymers (Callaghan *et al.*, 2000; Britton *et al.*, 1997; Tapadia *et al.*, 2006; Boukany *et al.*, 2008), micellar cubic phases (Eiser *et al.*, 2000), supra-molecular polymer solutions (van der Gucht *et al.*, 2006), transient networks (Michel *et al.*, 2001) and thermotropic side chain liquid crystal polymers (Robic *et al.*, 2002). Experiments indicate that gradient banding can also occur in hexagonal phases of surfactant solutions (Ramos *et al.*, 2000). Gradient banding where a shear-induced second phase is involved is observed in lamellar surfactant systems, where an "onion phase" is induced (Bonn *et al.*, 1998; Salmon *et al.*, 2003), in a semi-flexible thermotropic liquid crystalline polymer (mather *et al.*, 1997), where a nematic phase is induced by flow, and in poly-crystalline colloids (Chen *et al.*, 1992; Imhof *et al.*, 1994; Hunerbein *et al.*, 1996; Preis *et al.*, 1998), where crystals are shear-melted beyond some critical shear rate. For the onion system it is found that the location of the interface strongly fluctuates, the mechanism for which is still unclear (Salmon *et al.*, 2003). Interface fluctuations and periodic stress- and rate-response have been observed to accompany gradient banding in some cases (see, for example, (Lerouge *et al.*, 2006; Britton *et al.*, 1999; Salmon *et al.*, 2003; Callaghan *et al.*, 2000; Herle *et al.*, 2005; Lettinga *et al.*, 2009; Mannelville *et al.*, 2004; Hu *et al.*, 2002; Rofe *et al.*, 1996). A recent paper shows that the fluctuations in the interface are probably due the proximity of turbulence (Fardin *et al.*, 2010), while another recent paper by one of the present authors shows that the dynamical slip-stick phenomena are the result of a competition between slip and shear-band formation, which sets in at the lower shear rate of the stress plateau (Lettinga, 2009).

3. Strong Shear Thinning due to Entanglement Forces: Banding of Polymers

The van der Waals loop in Fig. 2 requires a very strong shear-thinning behaviour. In this section we briefly describe a mechanism that is relevant for entangled polymer systems. As far as we know, one of the first theories for polymers that explains a van der Waals type of behaviour of the standard stress as a function of shear rate was proposed in Ref. (McLeish *et al.*, 1986). The strong shear-thinning behaviour is due to shear-induced disentanglement. No shear-curvature (or stress-diffusion) contribution has been considered here, so that stationary states required the investigation of the stability of infinitely sharp interfaces between the bands (McLeish, 1987).

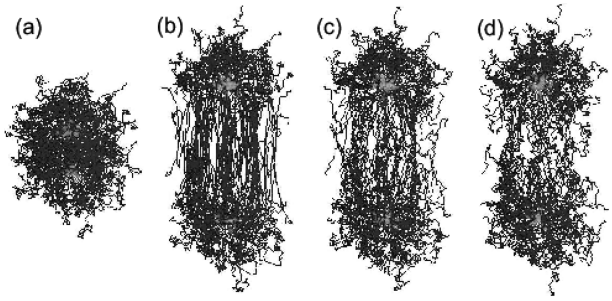

Fig. 3. A time-sequence of simulation snap-shots of two entangled star polymers. (a) Two star polymers at small core-to-core separation, where the polymer coronas are in equilibrium. (b) Overlapping coronas after an instantaneous displacement to a larger core-to-core separation. (c) and (d) depict the relaxation of the coronas to their new equilibrium state. Taken from Ref. (van den Noort, 2008).

An experimental system consisting of linear DNA has been shown to give rise to gradient banding as a result of entanglements (Ravindranath *et al.*, 2008). Similar to linear polymers, entanglements in star-like polymers (or “resin particles”), consisting of a small hard core and a corona of polymer arms, lead to gradient-shear banding. Simulations of gradient banding in star-polymer systems are reported in Ref.(van den Noort *et al.*, 2008). Since the coronas encompass many degrees of freedom, it is only feasible to perform simulations when an appropriate coarse graining of the dynamics of the coronas can be made. This is a highly non-trivial problem, since entanglements relax equally slow as the typical time scale on which the hard cores move. The coarse grained description proposed in Refs. (van den Noort *et al.*, 2007; 2008; Briels, 2009) is to describe the interaction between overlapping corona's with a single parameter n which measures the "number of entanglements". The corresponding inter-particle force F due to overlapping coronas is equal to,

$$F = \alpha\left[n - n_0(R)\right]\frac{dn_0(R)}{dR}, \tag{11}$$

with α a positive constant that characterizes the strength of entanglements and $n_0(R)$ the number of entanglements of two coronas when they are in equilibrium for a given distance R between the centers of the two particles. The equation of motion for the thermally averaged number of entanglements is,

$$\frac{dn}{dt} = -\frac{n - n_0(R)}{\tau}, \tag{12}$$

where the relaxation time τ measures the time scale on which entanglements evolve. The behaviour of two overlapping coronas is depicted in the computer-simulation images in Fig. 3 (van den Noort *et al.*, 2008). Two coronas in equilibrium at a short distance (Fig. 3a) are instantaneously

displaced to a larger core-to-core separation (Fig. 3b). After the instantaneous displacement, the number of entanglements is the same as before the displacement. According to eq. (11), this leads to an attractive entanglement force between the particles. Fig. 3c and d show the relaxation of the number of entanglements to the new equilibrium value, which is accompanied with a decrease of the entanglement forces between the particles. When two particles approach each other, there is a repulsive entanglement force.

These time-dependent, transient forces determine to a large extent the flow behaviour. The reason for strong shear thinning is that the coronas do not have time to develop entanglements when the shear rate is sufficiently large (such that $\dot{\gamma}\tau > 1$). Such a shear-induced reduction of interaction forces leads strong shear thinning, leading in turn to gradient banding, as found in computer simulations based on the above described coarse-grained description of entanglement forces (van den Noort *et al.*, 2008). In fact, the computer model can be cast into an analytical theory for the flow behaviour of systems where entanglements are important. This theory indeed predicts gradient banding and leads to an explicit expression for the shear-curvature viscosity (Briels *et al.*, 2011). This semi-microscopic model includes normal stresses and coupling to concentration, and identifies the mechanism that leads to mass fluxes as a result of spatial gradients in the shear rate which is at the basis of the SCC-instability that will be discussed in section 6.

The above mentioned semi-microscopic theory also applies to, for example, telechelic systems, where the number of entanglements is now the number of bridges and which indeed show shear-band formation (Sprakel *et al.*, 2008). Of course the specific form of n_0 as a function of R is now quite different from that of star-polymers, which affects the flow behaviour quite drastically.

4. Strong Shear Thinning due Critical Slowing Down: Banding of Wormlike Micelles

The proximity of an isotropic-nematic phase transition for suspensions of colloidal rods or worm-like micelles can lead to strong shear thinning. Near the isotropic-nematic (I-N) spinodal the orientational diffusion coefficient is small, so that there is little orientational Brownian motion that counteracts shear alignment. A quite small increase of the shear rate now leads to an appreciable increase in orientational order, which in turn leads to a significant decrease of the stress. Strong shear thinning due to shear alignment is pronounced in the vicinity to the isotropic-nematic spinodal, since the rotational diffusion coefficient tends to zero on approach of the spinodal. Formally, the dimensionless number that measures the importance of shear alignment relative to counter-balancing orientational diffusion is the effective rotational Péclet number $Pe_r^{eff} = \dot{\gamma}/D_r^{eff}$, with D_r^{eff} the effective rotational diffusion coefficient that includes the effects of rod-rod interactions. Close to the spinodal, where this diffusion coefficient is very small, a small increase of the shear rate results in a large increase of the rotational Péclet number, which implies the strong shear thinning mentioned above.

There are very few studies on systems that show gradient banding due to the proximity of the I-N spinodal. Recently Helgeson *et al.*. (Helgeson *et al.*, 2009) showed a connection between gradient banding and the I-N transition for a system of surfactant wormlike micelles, combining small angle light scattering and particle imaging velocimetry. In this section we describe experiments with poly(butadiene)-poly(ethylene oxide) (Pb-Peo) diblock copolymer with a 50–50 block composition in aqueous solution, which system was first introduced in Ref. (Won *et al.*, 1999), where it is also shown that this system exhibits an I-N phase transition. Here we will show that this system also displays gradient banding due to strong shear thinning as a result of the vicinity of the I-N spinodal (Lonetti *et al.*, 2008). The main advantage of this system is that the worms are quite stiff, with a persistence length of around 1 μm, they are quite long with a contour length of L=1 μm (though the system is polydisperse), while the worm diameter is 16 nm. As a result, the aspect ratio of L/d=63 is much larger as compared to common surfactant micellar systems, so that the diblock copolymer system shows an I-N transition at a modest concentration of about 1.7%, as will be seen later.

For a semi-quantitative interpretation of the experiments we will treat the system theoretically as a monodisperse hard-rod system. The stress tensor σ of a homogeneously sheared system of hard-core rods with a large aspect ratio can be expressed in terms of the orientational order-parameter tensor $\mathbf{S} = \langle \mathbf{uu} \rangle$, where $\mathbf{u}$ is the unit vector along the long axis of a rod, and the brackets $\langle \cdots \rangle$ denote ensemble averaging. The deviatoric part σ_D of the stress tensor of a homogeneously sheared suspension is given by (Doi *et al.*, 1986, Dhont *et al.*, 2003, 2006),

$$\sigma_D = 2\eta_0 \dot{\gamma} [\mathbf{E} + \frac{(L/d)^2}{3\ln\{L/d\}} \varphi \left\{ \Gamma \cdot \mathbf{S} + \mathbf{S} \cdot \Gamma - \mathbf{S}^{(4)} : \mathbf{E} - \frac{1}{3}\mathbf{I}\mathbf{S} : \mathbf{E} - \frac{1}{\dot{\gamma}} \frac{d\mathbf{S}}{dt} \right\}], \quad (13)$$

with η_0 the solvent viscosity, φ the volume fraction of rods, and $\hat{\Gamma}$ is the velocity-gradient tensor divided by the shear rate. In case of simple shear flow in the x-direction with y the gradient direction, the only non-zero component of the velocity gradient tensor is the xy-component which is equal to 1. Furthermore, $\mathbf{E} = \frac{1}{2}[\Gamma + \Gamma^T]$ is the symmetrized velocity-gradient tensor (where the superscript "T" stands for "transpose"), and $\mathbf{S}^{(4)} \equiv \langle \mathbf{uuuu} \rangle$ is a fourth-order polyadic tensor. A closure relation that expresses contractions of the form $\mathbf{S}^{(4)} : \mathbf{M}$ in terms of $\mathbf{S}$ for symmetric second rank tensors $\mathbf{M}$ is derived in Ref. (Dhont *et al.*, 2003, 2006),

$$\mathbf{S}^{(4)}:\mathbf{M}=\frac{1}{5}\big[\mathbf{S}\cdot\mathbf{M}+\mathbf{M}\cdot\mathbf{S}-\mathbf{S}\cdot\mathbf{S}\cdot\mathbf{M}-\mathbf{M}\cdot\mathbf{S}\cdot\mathbf{S}+2\mathbf{S}\cdot\mathbf{M}\cdot\mathbf{S}+3\mathbf{SS}:\mathbf{M}\big]. \quad (14)$$

This is a more accurate closure than the originally proposed closure by Doi and Edwards (Doi *et al.*, 1986). In Ref. (Forest *et al.*, 2003), an overview can be found of the different types of closures that have been devised. Equations (13,14) specify the stress in terms of the orientational order-parameter tensor, which is obtained from the equation of motion (Doi *et al.*, 1986, Dhont *et al.*, 2003, 2006),

$$\frac{d}{dt}\mathbf{S}=-6D_r\left[\mathbf{S}-\frac{1}{3}\hat{\mathbf{I}}-\frac{L}{d}\varphi\left\{\mathbf{S}\cdot\mathbf{S}-\mathbf{S}^{(4)}:\mathbf{S}\right\}\right] +\dot{\gamma}\{\Gamma\cdot\mathbf{S}+\mathbf{S}\cdot\Gamma^{T}-2\mathbf{S}^{(4)}:\mathbf{E}] \quad (15)$$

Here, D_r is the rotational diffusion coefficient of a single, non-interacting, freely diffusing rod. Solving this equation of motion numerically, and substitution of the solution into the expression (13) allows for a calculation of the stress of a suspension of rod-like hard-core particles, both in the linear and non-linear response-regime (Dhont *et al.*, 2003, 2006).

To illustrate orientational critical slowing down, consider the stability of the isotropic phase in the absence of flow, where $\mathbf{S}=\frac{1}{3}\mathbf{I}$, with $\mathbf{I}$ the identity. Substitution of $\mathbf{S}=\frac{1}{3}\mathbf{I}+\delta\mathbf{S}$ into eq.(15), using the closure relation (14), and linearization with respect to $\delta\mathbf{S}$ gives,

$$\delta\mathbf{S}(t):\ \exp\{-6D_r^{eff}t\}, \quad (16)$$

where the effective rotational diffusion coefficient is equal to (see the note at the end of the reference list),

$$D_r^{eff}=D_r\left[1-\frac{1}{5}\frac{L}{d}\varphi\right]. \quad (17)$$

For a volume fractions slightly smaller than the spinodal volume fraction $\varphi_s=5d/L$, the effective diffusion coefficient is small, which reflects the orientational critical slowing down discussed above. For volume fractions larger than φ_s, the effective rotational diffusion coefficient is negative. According to eq. (16) this implies that orientational order increases with time (details on the initial spinodal demixing kinetics is discussed in Ref. (Dhont, 1996)). Hence, the spinodal volume fraction marks the concentration where, upon increasing the concentration, the uniform isotropic state becomes unstable against the nematic state. With shear flow, the spinodal volume fraction depends on the shear rate, and can be obtained from numerical solutions of the above equations (Dhont *et al.*, 2003, 2006).

We observe from the flow curve of the worm-like diblock copolymer system as plotted in Fig. 4a (the solid lines) that this system displays significant shear thinning. Clearly the shear thinning for $[Pb-Peo]=2\,\%$ is more pronounced than for $[Pb-Peo]=1\,\%$ (we will use $[Pb-Peo]$ to denote the concentration of the $Pb-Peo$ micelles in weight percentage). The experiments discussed here indicate that the stronger shear thinning at the higher concentration is due to the vicinity of a spinodal point.

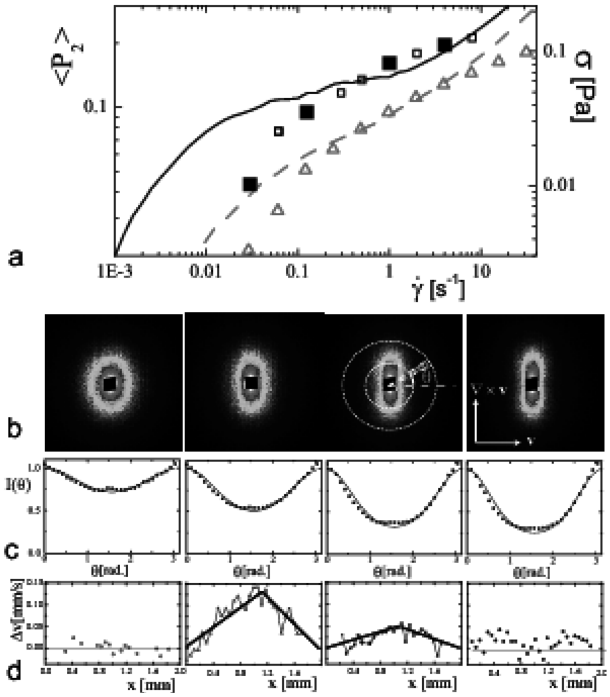

Fig. 4. (a) Flow curves (solid lines) and orientational order parameter (symbols) for $[Pb-Peo]=1\pm0.1\,\%$ (in red) and $[Pb-Peo]=2\pm0.1\,\%$ (in black) in deuterated water. The orientational order parameter is obtained from the small angle neutron scattering data in the flow-vorticity plane as shown in (b) for four overall shear rates ($\dot{\gamma}=0.03$, 0.1, 1 and 4 s) as indicated by the large filled symbols in (a). The total intensity within the region in between the two circles (indicated in the third figure) is used for the determination of the orientational order parameter distribution, which is given in the figures in (c). The solid lines are fits to $I(q,\theta)=\beta_0\exp\{\beta P_2(\theta)-1\}$, with β_0 and β the two fit parameters. (d) The relative flow velocity $\Delta v=v-\dot{\gamma}x$ for the same four overall shear rates. The solid lines are used to indicate the banded flow profile.

The orientational probability density function for Kuhn segments of the worms to attain an angle Θ with the flow direction are determined with *in situ* Small Angle Neutron Scattering (SANS). Scattered intensities are shown in Fig.4b in the flow-vorticity plane for four different overall shear rates. The orientational probability density function $P(\Theta)$ is assumed to have the form $:\exp\{\beta P_2(\cos\Theta)\}$, where β is an adjustable parameter and P_2 is the second order Legendre polynomial. The scattered intensity $I(q,\Theta)$ is proportional to the probability density function $P(\Theta)$ within the q-range where the intensity varies like $1/q$ (with q is the scattering wave vector). This scattering wave vector range is indicated by the two circles in the third scat-

tering pattern in Fig. 4b: in between these circles $I:1/q$. The corresponding length scale $2\pi/q$ is such that alignment of Kuhn segments of the chains is probed. The resulting (un-normalized) probability density functions are shown in Fig. 4c as a function of Θ, where the solid lines are fits the above mentioned exponential form. As expected, the probability is maximum for alignment along the flow direction and minimum for alignment along the vorticity direction. The scalar orientational order parameter $\langle P_2\rangle$, which is the largest eigen-value of the tensor $\mathbf{Q}\equiv\frac{3}{2}\left[\mathbf{S}-\frac{1}{3}\hat{\mathbf{I}}\right]$, with $\mathbf{I}$ the identity tensor, is obtained from numerical integration,

$$\langle P_2\rangle=\frac{\int_0^{\pi}\exp\{\beta P_2(\cos\theta)\}\,P_2(\cos\theta)\sin(\theta)d\theta}{\int_0^{\pi}\exp\{\beta P_2(\cos\theta)\}\sin(\theta)d\theta}. \qquad (18)$$

The value of $\langle P_2\rangle$ varies between zero (for an isotropic state) and unity (for a perfectly aligned nematic state). The order parameters measured with SANS are given in Fig. 4a by the symbols. As can be seen from Fig. 4a, the shear-thinning behaviour is accompanied by an increase of the order parameter, as expected.

Flow profiles in a Couette cell were measured by means of spatially resolved heterodyne light scattering. Four such profiles are plotted in Fig. 4d at the same shear rates as we used for the SANS patterns. We indeed find that shear banding for shear rates where the system is extremely shear thinning. Note however, that shear banding is not very pronounced in the sense that the difference in the shear rates within the two bands is not large. This is in accordance with a calculation for stiff rods with hard-core interactions (Dhont *et al.*, 2003), where even very close to the critical point only quite weak banding is predicted. The banding found here is more pronounced as compared to this theoretical prediction for stiff rods, probably because of chain-flexibility and polydispersity.

Since shear thinning can also in principle result from features that are specific for living polymers like scission and recombination of the worm-like structures, we still need to show that there is indeed an I-N phase transition close to the used concentrations, and that the shear-thinning mechanism is related to the distance from the spinodal. Already from visual observations between crossed polarizers it is known that this system undergoes a phase transition around the used concentrations. However, due to the fact that the system is polydisperse and well density matched, it is very difficult to obtain the isotropic and nematic binodal point through macroscopic phase separation experiments. As in an earlier paper (Lettinga *et al.*, 2004) we exploit here the large difference between the viscosity of the isotropic and nematic phase, leading to an increase of the stress in time when the system is quenched from a high shear-rate, where the nematic phase is stable, to a lower shear rate where the nematic phase becomes meta- or unstable. When phase separation occurs after a shear-rate quench to a particular shear rate, the measured stress increases with time. Thus, for each concentration the binodal shear rate $\dot{\gamma}_{bin}$ was determined as the shear rate at which the long-time increase of the measured shear stress σ_N after a quench vanishes (see top left plots in Fig. 5). The time-dependent (normalized) stress σ_N is obtained from fitted to $1-\Delta\sigma_N\exp\{-t/\tau\}$ with respect to the amplitude $\Delta\sigma_N$ and the time τ (data not shown). The binodal concentration for a given shear rate is the concentration where the amplitude $\Delta\sigma_N$ becomes zero (the red squares in the left plots in Fig. 5). The resulting binodal points are plotted in the central figure

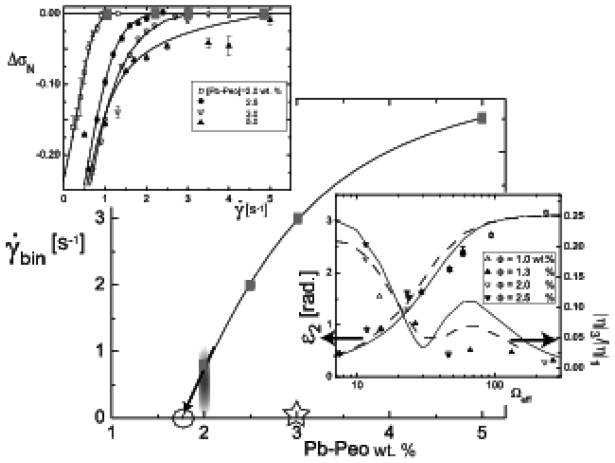

Fig. 5. Left top figure: Binodal points are obtained from the shear rate where the amplitude $\Delta\sigma_N$ of the time-dependent stress the binodal shear rates. Lines are guide to the eye. The main plot in the center is the non-equilibrium lower binodal in the shear-rate versus concentration plane. The circle indicates the equilibrium I-N binodal, that is, the binodal concentration in the absence of flow. The open star in the main figure indicates the experimentally obtained location of the spinodal at zero shear rate. The line is a guide to the eye, and represents the non-equilibrium binodal. The grey-shaded area is the shear-rate region where shear-banding is observed for the 2% sample. The bottom right plot shows exemplary the phase shifts ε_2 in the oscillatory response of $\langle P_2\rangle$, as well as the ratio of the leading order non-linear response function η_3 of the shear-stress (the third harmonic of the shear-stress), and the linear response function η_1, as a function of the effective Deborah number. The symbols indicate the experiments for different concentrations, as indicated in the figure. The solid lines are theoretical predictions for $\frac{L}{d}\varphi=10/3$, and the dashed line for $\frac{L}{d}\varphi=5/3$, based on numerical solutions of eqs.(13-15). For the calculation of the effective Deborah number (19) we used a value for the orientational diffusion coefficient at infinite dilution of $D_r=0.04s$ and $C=3.0$. The effective rotational Péclet number is taken equal to $Pe_r^{eff}=250$ for all data.

in Fig. 5 as a function of the shear rate. This figure constitutes the low-concentration branch of the non-equilibrium binodal for the Pb-Peo block copolymer system. The equilibrium I-N binodal concentration $[Pb-Peo] = 1.7 \pm 0.1$ % is found from an extrapolation to $\dot{\gamma}_{bin} \to 0$, and is marked in Fig. 5 by the large open circle.

The vertical shaded area in Fig. 5 indicates the shear-rate region where shear banding is observed for the 2% sample, which is very close to the lower binodal concentration. The location of the spinodal point is, however, more relevant for shear banding, since slowing down of orientational diffusion occurs on approach on this spinodal concentration. In order to find the spinodal point where the effective rotational diffusion coefficient is zero, we need to probe the dynamics of the system. A promising method to do that is by performing oscillatory shear experiments, and probe the response of orientational order with time-resolved SANS (t-SANS) and stress response with Fourier-transform rheology. These experiments can also be done with large oscillatory amplitudes, beyond the linear-response regime. Such experiments are referred to as Large Amplitude Oscillatory (LAOS-) experiments. In the right plot in Fig. 5, the phase angle shift ε_2 of the order parameter as obtained from such LAOS-experiments is plotted (the oscillating data), as well as the third harmonic η_3 divided by the first harmonic η_1 of the stress-response function (the monotonically increasing data), as a function of frequency. Here, the frequency is expressed in terms of the so-called effective Deborah number. This is the frequency ω of oscillation, dimensionalized by the effective rotational diffusion coefficient,

$$\Omega_{eff} = \omega / D_r^{eff}. \tag{19}$$

The (non-linear) response functions for different concentrations should superimpose when plotted against the effective Deborah number. The effective Deborah number is determined as follows. Since the volume fraction of rods enters the equation of motion (15) linearly, the effective rotational diffusion coefficient is also a linear function of concentration, similar to the diffusion coefficient in eq.(17). We therefore write,

$$D_r^{eff} = D_r \{1 - [Pb - Peo]/C\}, \tag{20}$$

where C is the concentration where the I-N spinodal is located. The concentration C is now chosen such that the various response functions for different concentrations superimpose when plotted against the effective Deborah number. A single value for C can indeed be found for which both the phase shift of the scalar orientational order parameter and the ratio η_3/η_1 superimpose for all four concentrations 1.0, 1.3, 2.0 and 2.5%, as can be seen in the plots on the right in Fig. 5. The spinodal concentration is thus found to be equal to 3.0%, and is indicated by the open star in Fig. 5. This point is inside the two-phase region, as it should.

Moreover, the experimental data for the non-linear response response (the phase shift ε_2 of the order parameter and the third-harmonic stress response in the right figure in Fig. 5) are semi-quantitatively in agreement with what is predicted from eqs.(13-15) (the solid line in the figure is for $\frac{L}{d}\varphi = 10/3$ and the dashed line for $\frac{L}{d}\varphi = 5/3$). The comparison with theory is only semi-quantitative since the theory neglects flexibility and polydispersity, as well as scission and recombination. LAOS-experiments (Cho, 2005) and FT-rheology (Wilhelm *et al.*, 1998) are increasingly popular, though often a theoretical basis for understanding of experimental results is missing (Cho, 2005). For a system of stiff rods that interact through a hard-core potential, eqs.(13-15) allow to calculate all the linear and non-linear response functions (Dhont *et al.*, 2003, 2006), which are in semi-quantitative agreement with the present system of rather stiff worm-like micelles.

5. Vorticity Banding

Vorticity banding has been observed in many different types of systems, like surfactant systems forming multilamellar vesicles ("onions") (Bonn *et al.*, 1998; Wilkins *et al.*, 2006), crystallizing colloids (Chen *et al.*, 1992), surfactant solutions (Fischer *et al.*, 2002), dispersions of semi-rigid, rod-like colloids (Dhont *et al.*, 2003; Kang *et al.*, 2006; 2008) and nanotube suspensions where flow-induced, highly elastic clusters are formed (Gibson *et al.*, 2004). The solid-like clusters in Ref. (Gibson *et al.*, 2004) align along the vorticity direction in a log-rolling state, probably in order to release the high elastic energy that would otherwise be stored in these clusters. The large scale bundles found in Ref. (Vermant *et al.*, 1999) in suspensions of sterically stabilized colloids indicate vorticity banding in these systems. The bands that are stacked along the vorticity direction (as sketched in the right Fig. 1) are visible either due to differences in optical birefringence (like for the rod-like colloids in Refs.(Dhont *et al.*, 2003, Kang *et al.*, 2006, 2008) and the onions in Ref. (Wilkins *et al.*, 2006)) or turbidity (like the worm-like micelles in Ref.(Fischer *et al.*, 2002). In a few of these systems (Chen *et al.*, 1992; Bonn *et al.*, 1998), a van der Waals loop in the stress is found, so that it seems that both gradient- and vorticity-banding can occur.

Experiments on fd-virus suspensions described in Refs. (Kang *et al.*, 2006; 2008) indicate that the origin of the vorticity-banding instability is related inhomogeneities. The non-equilibrium phase diagram of a fd-virus suspension (long and thin colloidal rods) is given in Fig. 6: the binodal closes at a certain critical shear rate, the two spinodals meet at the binodal below that shear rate (which might be called a non-equilibrium critical point), and there is a transition from shear alignment to tumbling (a detailed discussion of the phase behaviour of colloidal rods in flow can be found in Ref.(Ripoll *et al.*, 2008), where experi-

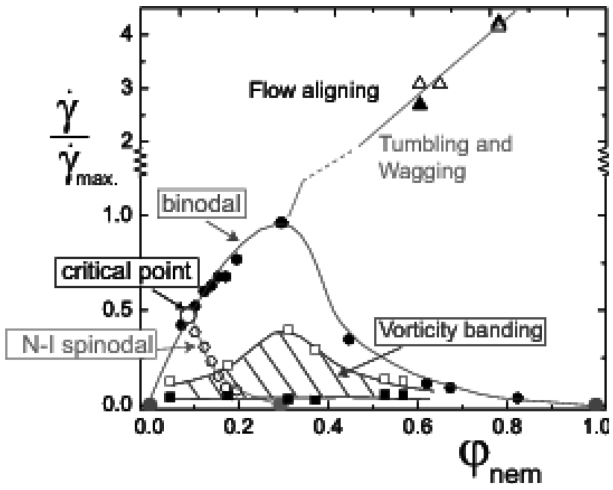

Fig. 6. The non-equilibrium phase diagram in the shear-rate versus concentration plane for a suspension of rod-like colloidal particles. The shaded area within the two-phase, isotropic-nematic coexistence region is the region where vorticity banding is observed. The shear rate is normalized with the shear rate $\dot{\gamma}_{max}$ where the maximum in the binodal occurs. The concentration is expressed in terms of the total fraction φ_{nem} of the nematic phase that is mixed with isotropic phase from a sample in isotropic-nematic equilibrium in the absence of flow. The data points are obtained by means of time-resolved rheology, light scattering and microscopy.

ments on fd-virus suspensions and simulations are presented). Moreover, within the shaded region, vorticity banding occurs. After some time (about an hour), a stationary, vorticity-banded pattern is formed that is visible between almost crossed polarizers.

After a quench from a high shear rate, where the system is in the one-phase region, into the shaded region in the phase diagram, first phase separation occurs where inhomogeneities are formed. When the system is sufficient inhomogeneous, vorticity bands develop. Note that vorticity banding only occurs within the two-phase region, so that it seems that he inhomogeneities are necessary for banding to occur. This is confirmed by measurements on the kinetics of band formation, where it is found that the kinetics is very different whether the inhomogeneities are formed through spinodal decomposition or nucleation-and-growth. A typical time dependence of the band height is given in Fig. 7a. Right after the shear-rate quench, the measured apparent band height decreases. This is due to the shear-induced elongation of the inhomogeneities that are formed during initial isotropic-nematic demixing. After about $10min$, however, the band height increases and regularly stacked vorticity bands are formed. It thus seems that a sufficient amount of inhomogeneities must be present before banding sets in. The growth of the vorticity band height can be described by a single exponential,

$$H(t) = H_0 + A[1 - \exp\{-(t - t_0)/\tau\}], \quad (21)$$

where H_0 is the apparent band height at the time t_0 where vorticity banding sets in, A is the total growth of the band height and τ is the growth time. Experiments have been performed (Kang *et al.*, 2006, 2008) for two fd-concentration: a lower concentration where spinodal decomposition occurs and a higher concentration where nucleation-and-growth occurs. The kinetics for these two concentrations is quite different. In case of spinodal decomposition, banding ceases to occur at the border shear rates (as indicated by the shaded region in Fig. 6 because the growth time diverges, while in case of nucleation-and-growth banding ceases to occur because the amplitude A vanishes at the border shear rates. This shows that the mechanical properties of the inhomogeneities, which are different for the case of spinodal decomposition and nucleation-and-growth, play an essential role in the vorticity-banding instability. In the (quasi-) stationary state, inhomogeneities are still present within the vorticity bands, and the bands disappear as soon as these inhomogeneities are not present: inhomogeneities slowly sediment and are not present at the top of the sample anymore after some time, while at the same time bands also disappear (Kang *et al.*, 2006). Moreover, particle-tracking experiments reveal a rolling fluid flow within the bands. In Fig.7b, the z-coordinate (along the vorticity direction) of the tracer particle within a band as a function of time is plotted. As can be seen, there is an oscillatory motion in the vorticity direction. The particle slowly sediments, giving rise to the overall decrease of the z-position in Fig. 7b. The oscillatory motion of the tracer particle indicates that the bands are in internal rolling motion.

These observations lead to the proposition that the vorticity-banding instability is an elastic instability (Kang *et al.*, 2006, 2008), similar to the Weissenberg effect in polymer systems. The microscopic origin of the Weissenberg effect in polymer systems is well-known (Pakdel *et al.*, 1996; Groisman *et al.*, 1998), and is similar to elastic instabilities that are discussed in Refs. (Muller *et al.*, 1989; Larson *et al.*, 1990; Shaqfeh *et al.*, 1992; 1996). A polymer chain in a flow with gradients in the shear rate, like in the gap of a Couette cell, will be non-uniformly stretched. The resulting restoring forces on fluid elements act along the gradient direction, and give rise to normal stresses that can lead to fluid flow along the gradient direction. Such an flow gives rise to the observed rolling flow in bands stacked along the vorticity direction. Instead of the polymer chains, we now have the inhomogeneities that are formed during the initial stages of phase separation which are similarly non-uniformly, elastically stretched. The vorticity instability is therefore proposed to be due to the Weissenberg effect, where the role of polymer chains is now played by inhomogeneities. Indeed, for the systems mentioned above that

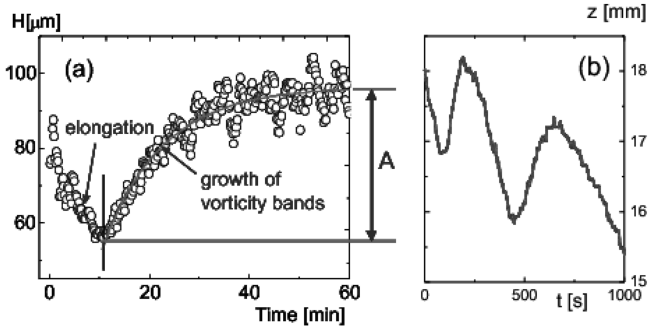

Fig. 7. (a) The measured band height as a function of time. The red line through the data points is a fit to eq.(21). (b) The position of a tracer sphere, within a band, along the vorticity direction in the stationary state as a function of time. The band height in this particle-tracking experiment is much larger than for the experiments in (a), due to the addition of more Dextran that serves as a depletant, which renders the rods effectively attractive.

exhibit vorticity banding, such inhomogeneities can be identified. For example, in case of the worm-like micellar systems, the worms themselves act as the elastically deformable inhomogeneities (Fardin *et al.*, 2010).

Vorticity banding is in some cases observed when discontinuous (or very strong) shear thickening occurs (like for the worm-like micelles in Refs. (Bonn *et al.*, 1998; Wilkins *et al.*, 2006; Fischer *et al.*, 2002), where the shear stress exhibits a (quasi-) discontinuity, and jumps at a given shear rate to a higher value. Such a very strong shear-thickening behaviour is probably due to the shear-induced formation of a new, viscous phase. In Ref. (Fischer *et al.*, 2002) there are indeed clear indications for such a shear-induced new phase. Also for crystalline colloids there are indications of a shear-induced new phase that gives rise to vorticity banding (Chen *et al.*, 1992). The formation of such shear-induced new phases are accompanied by the formation of inhomogeneities. These inhomogeneities could then give rise to hoop stresses which lead to vorticity banding through the Weissenberg scenario as discussed above (personal communication with John Melrose). A recent proposition (Fielding, 2007) is that normal stresses can be generated within the interface in a gradient-banded state, giving rise to vorticity banding. In this scenario, a gradient-banded structure is formed prior to the vorticity bands. Vorticity banding is indeed some times found to occur in conjunction with a van der Waals loop in the stress, like for the multi-lamellar vesicles in Ref. (Bonn *et al.*, 1998) and the colloidal crystals in Ref. (Chen *et al.*, 1992).

6. The Shear-Gradient Concentration Coupling (SCC-) Instability

Here we consider an instability where coupling to concentration is essential. When such a coupling is important, a coupled diffusion equation and Navier-Stokes equation should be considered. A linear stability analysis of such a coupled diffusion and Navier-Stokes equation has been performed by Schmitt *et al.*. in Ref. (Schmitt *et al.*, 1995). This analysis shows that coupling to concentration can lead to an instability even when $d\sigma(\dot{\gamma}_0)/d\dot{\gamma}_0$ is positive. In order to analyze the effect of coupling to concentration on the initial instability of the flow, Fick's diffusion equation is first generalized to include driving forces for mass transport due to gradients in the shear rate. For small gradients in concentration, the mass flux $\mathbf{j}$ can be written as $\mathbf{j} = \rho\mathbf{u} - M\nabla\mu$, with ρ the concentration, $\mathbf{u}$ the flow velocity, μ the chemical potential and M a positive transport coefficient. The chemical potential is a function of density and local shear rate: $\mu \equiv \mu(\dot{\gamma}, \rho)$. In principle, such a shear-rate dependent chemical potential is ill-defined, since shear flow is a non-conservative external field (it is explicitly shown by computer simulations in Ref. (Butler *et al.*, 2002) that coexistence between crystals and fluid in flow can not be described by means of a chemical potential). One possible way, however, to formally define a shear-rate dependent chemical potential is to substitute shear-rate dependent order parameters into a known expression for the chemical potential. For example, in an expression for the chemical potential for rod-like colloids, one can simply substitute the shear-rate dependent orientational order parameter, where its shear-rate dependence is obtained from independent equations of motion. It is not known how accurate such descriptions are. Assuming a shear-rate dependent chemical potential, the mass flux is thus formally written as,

$$\mathbf{j} = \rho\mathbf{u} - M\left[\frac{\partial\mu(\dot{\gamma},\rho)}{\partial\rho}\nabla\rho + \frac{\partial\mu(\dot{\gamma},\rho)}{\partial\dot{\gamma}}\nabla\dot{\gamma}\right]. \tag{22}$$

The fluid flow velocity is assumed to be in the x-direction. Only the magnitude of the velocity is allowed to vary, not its direction. Moreover, its magnitude is assumed to vary only in the gradient direction (the y-direction). Variations in the vorticity direction need not be considered, since the interest here is in instabilities extending along the gradient direction. Hence, the component u of the velocity in the x-direction is written, as before, as $u(y,t) = \dot{\gamma}_0 y + \delta u(y,t)$, where $\dot{\gamma}_0$ is the applied shear rate. Similarly, the density is assumed to vary only along the gradient direction : $\rho(y,t) = \rho_0 + \delta\rho(y,t)$, with ρ_0 the constant, initial concentration. Substitution of these expressions for the velocity and concentration into the expression for the flux and linearization with respect to δu and $\delta\rho$ leads to the diffusion equation,

$$\frac{\partial\delta\rho(y,t)}{\partial t} = D\frac{\partial^2\delta\rho(y,t)}{\partial y^2} + M\frac{\partial\mu(\dot{\gamma}_0,\rho_0)}{\partial\dot{\gamma}_0}\frac{\partial^3\delta u(y,t)}{\partial y^3}, \tag{23}$$

where it used that the local shear rate is equal to $\dot{\gamma} = \partial u(y,t)/\partial y$. Furthermore,

$$D = M\frac{\partial\mu(\dot\gamma_0,\rho_0)}{\partial\rho_0}, \tag{24}$$

is Fick's diffusion coefficient. Since the interest here is only in variations in the y-direction of the flow component u in the x-direction, the only component of the stress tensor $\mathbf{S}$ that contributes is $\sigma\equiv\sum_{yx}$ (apart from an irrelevant contribution $\sum_{xx}$). Here we assume that the shear stress is given by the standard stress σ, which is now not just a function of the local shear rate, as in the minimal model, but also of the concentration. To leading order in $\delta\dot\gamma$ and $\delta\rho$, the deviation of the stress tensor from its initial value is thus given by,

$$\delta\sigma = \frac{\partial\sigma(\dot\gamma_0,\rho_0)}{\partial\dot\gamma_0}\delta\dot\gamma + \frac{\partial\sigma(\dot\gamma_0,\rho_0)}{\partial\rho_0}\delta\rho, \tag{25}$$

where the indices "0" refer to the homogeneously sheared system, before banding occurred. The linearized Navier-Stokes equation thus reads (as before, ρ_m is the mass density of the fluid),

$$\rho_m\frac{\partial\delta u(y,t)}{\partial t} = \frac{\partial\sigma(\dot\gamma_0,\rho_0)}{\partial\dot\gamma_0}\frac{\partial^2\delta u(y,t)}{\partial y^2} + \frac{\partial\sigma(\dot\gamma_0,\rho_0)}{\partial\rho_0}\frac{\partial\delta\rho(y,t)}{\partial y}. \tag{26}$$

Equations (23,26) were derived in a somewhat more general setting in Ref. (Schmitt *et al.*, 1995). Here we restrict ourselves to variations extending along the y-direction only.

Disregarding the finite extent of the shear-cell gap width, the analysis for stability of variations along the gradient direction can be performed by substitution of,

$$\begin{aligned}\delta u(y,t) &= \delta u_0\exp\{iky-\Gamma t\},\\ \delta\rho(y,t) &= \delta\rho_0\exp\{iky-\Gamma t\},\end{aligned} \tag{27}$$

where δu_0 and $\delta\rho_0$ are the initial amplitudes of the perturbations of the velocity and concentration, respectively. Clearly, both the density and velocity are unstable when $\Gamma<0$. A finite gap width would require to write these variations as a sine/cosine-series with quantized wave vectors, as was done in the section on the minimal model. This is a technicality that would unnecessarily complicate the analysis in the present case. Substitution of eqs.(27) into eqs.(23,26) gives,

$$\begin{aligned}\Gamma\delta\rho_0 &= Dk^2\delta\rho_0 + ik^3M\frac{\partial\mu(\dot\gamma_0,\rho_0)}{\partial\dot\gamma_0}\delta u_0,\\ \rho_m\Gamma\delta u_0 &= k^2\frac{\partial\sigma(\dot\gamma_0,\rho_0)}{\partial\dot\gamma_0}\delta u_0 - ik\frac{\partial\sigma(\dot\gamma_0,\rho_0)}{\partial\rho_0}\delta\rho_0.\end{aligned} \tag{28}$$

Eliminating $\delta\rho_0$ from the second equation gives a second order equation for Γ,

$$\begin{aligned}&\Gamma^2 - \Gamma\frac{k^2}{\rho_m}\left(\rho_m D + \frac{\partial\sigma(\dot\gamma_0,\rho_0)}{\partial\gamma_0}\right)\\ &+\frac{k^4}{\rho_m}\left(D\frac{\partial\sigma(\dot\gamma_0,\rho_0)}{\partial\dot\gamma_0} - M\frac{\partial\mu(\dot\gamma_0,\rho_0)}{\partial\dot\gamma_0}\frac{\partial\sigma(\dot\gamma_0,\rho_0)}{\partial\rho_0}\right)=0.\end{aligned} \tag{29}$$

It follows from this result that Γ is negative when (Schmitt *et al.*, 1995),

$$D\frac{\partial\sigma(\dot\gamma_0,\rho_0)}{\partial\dot\gamma_0} < M\frac{\partial\mu(\dot\gamma_0,\rho_0)}{\partial\dot\gamma_0}\frac{\partial\sigma(\dot\gamma_0,\rho_0)}{\partial\rho_0}. \tag{30}$$

When there is no coupling to concentration, that is, when $\partial\sigma(\dot\gamma_0,\rho_0)/\partial\rho_0=0$, this implies an instability either when (i) $D<0$ and $\partial\sigma(\dot\gamma_0,\rho_0)/\partial\dot\gamma>0$, or (ii) $D>0$ and $\partial\sigma(\dot\gamma_0,\rho_0)/\partial\dot\gamma_0<0$. Case (i) corresponds to a spinodal instability leading to phase separation driven by thermodynamic forces, and case (ii) corresponds to the mechanical gradient-banding instability that was discussed within the minimal model discussed in section 2. *When there is coupling to concentration, that is, when* $\partial\sigma(\dot\gamma_0,\rho_0)/\partial\rho_0\neq0$, *there can be an instability even though* D *and* $\partial\sigma(\dot\gamma_0,\rho_0)/\partial\dot\gamma_0$ *are positive*. This is an instability that is purely driven by coupling with concentration and is absent within the minimal model.

The intuitive explanation of this shear-gradient concentration coupling (SCC-) instability is as follows. When $\partial\mu(\dot\gamma_0,\rho_0)/\partial\dot\gamma_0>0$ there will be mass transport in the direction of lower shear rates (as can be seen from eq.(22)). In a Couette cell, mass will be transported to the outer cylinder. When in addition $\partial\sigma(\dot\gamma_0,\rho_0)/\partial\rho_0>0$, the shear rate near the outer cylinder to which mass is transported will decrease, since the system will try to regain mechanical equilibrium where the shear stress is constant throughout the gap. Such a decrease in shear rate will lead to larger spatial gradients in the shear rate and thus enhances mass transport towards the outer cylinder. This self-amplifying mechanism leads to a high concentration and low shear-rate region near the outer cylinder, and a low concentration and high shear-rate region near the inner cylinder.

The self-amplifying mechanism is counter balanced by diffusion and a possible strong decrease of the stress on decreasing the shear rate. Diffusion will drive the system back to the homogeneous state and thus counter balances mass transport to regions with lower local shear rates. If the stress strongly decreases with decreasing shear rate, that is, when $\partial\sigma(\dot\gamma_0,\rho_0)/\partial\dot\gamma_0$ is positive and large, the decrease of the local shear rate in regaining mechanical equilibrium is small. This explains why the right hand-side in eq.(30) ("the driving force for the instability") should be larger than the left hand-side ("the counter-balancing forces"). When both derivatives on the right hand-side in eq.(30) are negative, the same mechanism is at work, where now mass is transported to regions of higher shear rate.

It is not clear yet whether the SCC-instability leads to a stationary gradient-banded state in the sense that regions (the "bands") exist within which the shear rate is essentially constant, independent of position. In any case, a stationary state is reached when gradients in concentration are sufficiently large so that Fickian diffusion counter balances the above mentioned driving force for mass transport con-

nected to the shear-rate dependence of the chemical potential. In order to establish whether true shear-banded states are formed in the stationary state, the appropriate Navier-Stokes equation and diffusion equation should be solved numerically. To describe the stationary state, the Navier-Stokes equation must include the shear-curvature contribution in order to stabilize the system against the initial, rapid formation of large gradients in the flow velocity. When gradients in concentration are large, a similar higher order derivative in the concentration ($\partial^4\rho(y,t)/\partial y^4$) should be added to the diffusion equation. Such a higher order derivative was first introduced by Cahn and Hilliard in their analysis of the initial stages of spinodal decomposition (in which case D is negative) (Cahn *et al.*, 1958, 1959)(a microscopic derivation of the Cahn-Hilliard theory based of the Smoluchowski equation is given in Ref. (Dhont, 1996). The coefficient complying with this higher order derivative is referred to as the *Cahn-Hilliard square-gradient coefficient*, which plays the same role as the shear-curvature viscosity in the sense that it stabilizes the system against rapid formation of very large spatial gradients. So far, no attempt has been made to analyze the stationary states that result from the SCC-instability.

Other degrees of freedom that strongly couple to the shear viscosity can play a similar role as concentration. For example, for worm-like micelles and rod-like colloids, orientational order can be important. Coupling to concentration *and* orientational order is discussed in Refs. (Olmsted *et al.*, 1997; 1999). Coupling of flow to the non-conserved composition of a binary mixture, where one of the components only exist under flow conditions, is discussed in Ref. (Goveas *et al.*, 2001). Such a shear-induced new component that couples to the stress can lead to banding, depending on whether the stress or overall shear rate is controlled. In case of worm-like micelles, part of the high shear-rate branch, following the van der Waals loop, can be unstable due to coupling to the average worm length (Fielding *et al.*, 2004). A similar self-amplifying effect as for concentration coupling discussed above may be responsible for such an instability. Since now part of the high shear-rate band is in itself unstable, there is no stationary gradient-banded state. This leads to time-dependent flow profiles under stationary applied shear rates (Fielding *et al.*, 2004).

One of the possible reasons why the SCC-instability has not been further considered after the original publication by Schmitt (Schimitt *et al.*, 1995) might be that the origin of the shear-rate dependence of the chemical potential is unclear. Here we will show that shear-gradient induced mass transport is coupled to the shear-induced distortion of the pair-correlation function. First of all, the diffusion equation reads,

$$\frac{\partial\rho}{\partial t}+\nabla\cdot\left[\rho\mathbf{u}\right]=D_0\nabla^2\rho-\beta D_0\nabla\cdot\mathbf{B}, \tag{31}$$

where D_0 is the free diffusion coefficient, while interactions between particles are included through the body force $\mathbf{B}$, which, with the neglect of hydrodynamic interactions, is equal to,

$$\mathbf{B}(\mathbf{r},t)=-<\sum_{i=1}^{N}\left[\nabla_i\Phi\right]\delta(\mathbf{r}-\mathbf{R}_i)>(t), \tag{32}$$

with Φ the interaction potential between colloidal particles, and δ is the delta-distribution with $\boldsymbol{R}_i$ the position coordinate of colloid i. The eqs.(31,32) can be derived from the Smoluchowski equation, which is discussed in detail in Ref. Briels (2011). The first term on the right hand-side in the equation of motion (31) describes the evolution of the density due to *free* diffusion, in the absence of colloid-colloid interactions, while the second term accounts for mass transport due to interactions between the colloids. In fact, the diffusion equation (31) implies a flux equal to,

$$\mathbf{j}=\rho\mathbf{v}=\rho\mathbf{u}+\frac{\rho}{\zeta}\left[-k_BT\nabla\ln\rho+\frac{\mathbf{B}}{\rho}\right], \tag{33}$$

with $\mathbf{v}$ the velocity of a colloid, where it is used that $D_0=k_BT/\zeta$, with ζ the single-particle friction coefficient. This equation expresses force balance on the Smoluchowski time scale, where the friction force $-\zeta\mathbf{v}$ is balanced by sum of the Brownian force $-k_BT\nabla\ln\rho$ and the interaction force per colloid $\mathbf{B}/\rho$. In the absence of flow, the body-force contribution can be shown to have the form $\Delta D\nabla^2\rho$ (see, for example, Ref.(Dhont 1996). The free-diffusion contribution and the colloid-colloid interaction contribution can thus be lumped into a single term of the form $D^{eff}\nabla^2\rho$, where $D^{eff}=D+\Delta D$, which renders eq.(31) identical to Fick's law. As will be discussed later, the interaction contribution ΔD also contains other types of terms in the presence of flow. The Navier-Stokes equation for the flow velocity can be written as,

$$\rho_m\left\{\frac{\partial\mathbf{u}}{\partial t}+\mathbf{u}\cdot\nabla\mathbf{u}\right\}=\mathbf{B}, \tag{34}$$

which is supplemented by the incompressibility equation,

$$\nabla\cdot\mathbf{u}=0. \tag{35}$$

We will now show how the expression (32) for the body force gives rise to the term $:\nabla\dot{\gamma}$ in eq.(22) for the mass flux. First of all, the ensemble average in eq.(32) is written in terms of an integral with respect to the probability density function P_N of the position coordinates of all colloids,

$$\mathbf{B}(\mathbf{r},t)=-N\int d\mathbf{R}_1\cdots\int d\mathbf{R}_N\ P_N\nabla_1\Phi\ \delta(\mathbf{r}-\mathbf{R}_1). \tag{36}$$

For a potential Φ that is a pair-wise additive sum of pair-interactions, with V the pair-interaction potential, this readily leads to,

$$\mathbf{B}(\mathbf{r},t)=-N(N-1)\int d\mathbf{R}_2\ P_2(\mathbf{r},\mathbf{R}_2,t)\nabla V(|\mathbf{r}-\mathbf{R}_2|), \tag{37}$$

where,

$$P_2(\mathbf{R}_1,\mathbf{R}_2,t)=\int d\mathbf{R}_3\cdots\int d\mathbf{R}_N\; P_N(\mathbf{R}_1,\mathbf{R}_2,\mathbf{R}_3,\cdots,\mathbf{R}_N,t). \quad (38)$$

Introducing the pair-correlation function,

$$P_2(\mathbf{r},\mathbf{R}_2,t)=\frac{1}{N(N-1)}\rho(\mathbf{r},t)\rho(\mathbf{R}_2,t)g(\mathbf{r},\mathbf{R}_2,t,[\rho,\dot\gamma]), \quad (39)$$

where the notation $[\rho,\dot\gamma]$ is used to indicate functional dependence on the density and shear rate for an inhomogeneous system, the body force is written as,

$$\mathbf{B}(\mathbf{r},t)=-\rho(\mathbf{r},t)\int d\mathbf{R}_2\;\rho(\mathbf{R}_2,t)g(\mathbf{r},\mathbf{R}_2,t,[\rho,\dot\gamma])\nabla V(|\mathbf{r}-\mathbf{R}_2|). \quad (40)$$

Since the potential restricts the integration range to distances $|\mathbf{r}-\mathbf{R}_2|$ less than the range R_V of the pair-interaction potential, only the short-ranged shear-induced distortion of the pair-correlation need be considered. For these microscopic distances this distortion is to a good approximation affine, so that,

$$g(\mathbf{r},\mathbf{R}_2,t,[\rho,\dot\gamma])=g^{eq}(\mathbf{r},\mathbf{R}_2,[\rho,\dot\gamma])+g_0(\mathbf{r},\mathbf{R}_2,t,[\rho,\dot\gamma]) +\frac{\mathbf{r}-\mathbf{R}_2}{|\mathbf{r}-\mathbf{R}_2|}\cdot\hat{\mathbf{E}}\cdot\frac{\mathbf{r}-\mathbf{R}_2}{|\mathbf{r}-\mathbf{R}_2|}g_1(\mathbf{r},\mathbf{R}_2,t,[\rho,\dot\gamma]), \quad (41)$$

where is the equilibrium pair-correlation function (in the absence of shear flow), g_0 is the isotropic shear-induced distortion and g_1 the anisotropic distortion of the pair-correlation function. Furthermore, $\mathbf{E}$ is the symmetric part of the velocity-gradient tensor divided by the local shear rate. For a simple shear flow in the x-direction with y the flow direction, the only two non-zero entries for $\mathbf{E}$ are the xy and yx entries, which are equal to $1/2$. Since the shear rate and density vary very little over the small distances less than R_V under consideration, the density $\rho(\mathbf{R}_2,t)$ can be Taylor expanded around $\mathbf{r}$ to leading order in gradients,

$$\rho(\mathbf{R}_2,t)=\rho(\mathbf{r},t)+(\mathbf{R}_2-\mathbf{r})\cdot\nabla\rho(\mathbf{r},t). \quad (42)$$

Furthermore, the various contributions to the pair-correlation functions are approximately equal to the pair-correlation function in eq.(41) in an isotropic system, with homogeneous density and shear rate, but with a density and shear rate in between the positions $\mathbf{r}$ and $\mathbf{R}_2$. For example,

$$g_0(\mathbf{r},\mathbf{R}_2,t,[\rho,\dot\gamma])=\bar g_0(|\mathbf{r}-\mathbf{R}_2|,\bar\rho,\bar{\dot\gamma}),$$
$$\text{with}\quad \bar\rho=\rho\left(\frac{1}{2}(\mathbf{r}+\mathbf{R}_2),t\right)\quad\text{and}\quad \bar{\dot\gamma}=\dot\gamma\left(\frac{1}{2}(\mathbf{r}+\mathbf{R}_2),t\right), \quad (43)$$

and similar for g^{eq} and g_1. Here, the overbar on g_0 indicates that this is the correlation function of a system with homogeneous density and shear rate equal to $\bar\rho$ and $\bar{\dot\gamma}$, respectively. Note that the time dependence of the pair-correlation function is entirely due to the time dependence of the density and shear rate: since the time-evolution of the macroscopic density and shear rate are much slower that the relaxation time of the pair-correlation function for short distances less than R_V, the pair-correlation function adjusts itself essentially instantaneously to its local stationary form. Within a leading order gradient expansion, it is thus found that,

$$g_0(|\mathbf{r}-\mathbf{R}_2|,t,[\rho,\dot\gamma])=\bar g_0(R|\rho,\dot\gamma)+\frac{1}{2}\frac{\partial\bar g_0(R|\rho,\dot\gamma)}{\partial\rho}\mathbf{R}\cdot\nabla\rho +\frac{1}{2}\frac{\partial\bar g_0(R|\rho,\dot\gamma)}{\partial\dot\gamma}\mathbf{R}\cdot\nabla\dot\gamma, \quad (44)$$

and similar for g^{eq} (for which the shear-rate dependence is of course absent) and g_1, where $\mathbf{R}=\mathbf{R}_2-\mathbf{r}$, and where ρ and $\dot\gamma$ are now understood to denote the local density and shear rate (omitting the now superfluous overbar notation). Substitution of eqs.(42,44) into eq.(40) for $\mathbf{B}$, and performing the angular integrations gives,

$$\mathbf{B}(\mathbf{r},t)=-\left[\frac{\partial P_0(\rho,\dot\gamma)}{\partial\rho}-k_BT\right]\nabla\rho-\frac{\partial P_0(\rho,\dot\gamma)}{\partial\dot\gamma}\nabla\dot\gamma -\frac{\partial P_1(\rho,\dot\gamma)}{\partial\rho}\mathbf{E}\cdot\nabla\rho-\frac{\partial P_1(\rho,\dot\gamma)}{\partial\dot\gamma}\mathbf{E}\cdot\nabla\dot\gamma, \quad (45)$$

up to leading order in spatial gradients, where,

$$P_0(\rho,\dot\gamma)=\rho k_BT-\frac{2\pi}{3}\rho^2\int_0^\infty dR\;R^3\frac{dV(R)}{dR}\left[g^{eq}(R|\rho)+\bar g_0(R|\rho,\dot\gamma)\right], \quad (46)$$

and,

$$P_1(\rho,\dot\gamma)=-\frac{4\pi}{15}\rho^2\int_0^\infty dR\;R^3\frac{dV(R)}{dR}\bar g_1(R|\rho,\dot\gamma). \quad (47)$$

As before, ρ and $\dot\gamma$ are understood to be the local density and shear rate, which are functions of position $\mathbf{r}$ and time t. Equation (45) can also be written as,

$$\mathbf{B}(\mathbf{r},t)=-\nabla\left[P_0(\rho,\dot\gamma)-\rho k_BT\right]-\hat{\mathbf{E}}\cdot\nabla P_1(\rho,\dot\gamma). \quad (48)$$

Note that with the neglect of shear-induced changes of the pair-correlation, in which case $\bar g_0$ vanishes, eq.(46) is nothing but the pressure. From eq.(48) it is readily verified that only the body force $-\nabla[P_0-\rho k_BT]$ acts along the gradient direction. According to eqs.(33,45), the mass flux in the gradient direction is thus equal to,

$$\mathbf{j}=\rho\mathbf{u}-\beta D_0\nabla P_0(\rho,\dot\gamma) =\rho\mathbf{u}-\beta D_0\left[\frac{\partial P_0(\rho,\dot\gamma)}{\partial\rho}\nabla\rho-\frac{\partial P_0(\rho,\dot\gamma)}{\partial\dot\gamma}\nabla\dot\gamma\right]. \quad (49)$$

This is precisely the form for the flux in eq.(22) that was postulated by Schmitt (Schmitt *et al.*, 1995). In the absence of flow, where P_0 is just the equilibrium pressure P^{eq}, it follows from the Gibbs-Duhem relation $\partial P^{eq}/\partial\rho=\rho\partial\mu/\partial\rho$ that the kinetic coefficient M in Schmitt's expression (22) for the flux should be identified as $M=\beta\rho D_0$. More importantly, the above analysis shows that one should formulate the flux in terms of a "generalized pressure" instead of a "generalized chemical potential". The generalized pressure is simply the pressure obtained from the standard expres-

sion for the equilibrium pressure,

$$P^{eq}(\rho) = \rho k_B T - \frac{2\pi}{3}\rho^2 \int_0^\infty dR\, R^3 \frac{dV(R)}{dR} g^{eq}(R|\rho), \qquad (50)$$

by replacing the equilibrium pair-correlation function g^{eq} by the shear-distorted pair-correlation function.

The above analysis may serve as a starting point for a further (semi-) microscopic development of the SCC-instability, and in particular for an investigation of the resulting stationary state velocity profile. It could very well be that the SCC-instability results in a banded state that is very similar to that for gradient-banding that was discussed in section 2.

7. Summary and Conclusions

In this overview, a minimal model is presented that describes the basic features of gradient banding. The constitutive equation in this model is straightforwardly obtained from the usual formal expansion of the stress tensor with respect to gradients in the flow velocity, extending it to include the second order term. The proportionality constant of the leading term in this gradient expansion is the shear viscosity while the proportionality constant for the second term is referred to as "the shear-curvature viscosity". The second order term is necessary to describe the strong spatial variations within the interface between the two bands. The minimal model predicts that, in the absence of coupling to concentration, no banding can occur under controlled stress conditions, it gives rise to a banded state in the stationary state under controlled shear-rate conditions where the shear rates within the bands are constant, and it leads a stress selection rule. A necessary feature for gradient banding is strong shear-thinning behaviour. A brief discussion of transient entanglement forces is given, which lead to strong shear thinning (a much more detailed account on transient entanglement forces and resulting constitutive equations will be given in a future publication (Briels *et al.*, 2011)). Experiments are presented which show that shear thinning in a worm-like micellar system due to the vicinity of the isotropic-nematic spinodal is sufficiently strong to give rise to gradient banding.

Vorticity banding has a completely different origin than gradient banding. On the basis of experiments on fd-virus suspensions (very long and thin colloidal rods), it seems likely that the vorticity banding instability is an elastic instability. Here, inhomogeneities are non-uniformly deformed in flows that exhibit gradients in the shear rate (like in a Couette cell), giving rise to non-uniform normal stresses along the gradient direction that set the suspension into motion. In case of the fd-virus suspensions, the inhomogeneities are due to initial isotropic-nematic phase separation, while for worm-like micelles the worms themselves serve as the necessary inhomogeneities. The vorticity-banding instability is thus related to the Weissenberg effect for polymer systems, where the role of polymer chains is now played by inhomogeneities.

The most important omission in the minimal model for gradient banding is coupling to concentration. As Schmitt already described in Ref. (Schmitt *et al.*, 1995), strong coupling to concentration can lead to an instability without shear thinning. We referred to this instability here as the shear-gradient concentration coupling (SCC-) instability. Schmitt formulated the instability in terms of a shear-rate dependent "generalized chemical potential". The phenomenology of this instability is discussed, and a microscopic basis is given for Schmitt's generalized chemical potential. It is shown that the mass flux driven by shear-gradients should not be formulated in terms of a chemical potential, but rather in terms of a "generalized pressure", which is obtained from the equilibrium expression for the pressure with the pair-correlation function replaced by the shear-distorted pair-correlation function. It is still not known what the stationary velocity profile will be when the SCC-instability occurs.

References

Berret J. -F., 2005, in Molecular Gels (eds. Weiss RG, Terech P), Rheology of wormlike micelles: Equilibrium properties and shear banding transition, Springer, Dordrecht, 235-275.

Berret J. -F., G. Porte and J. -P. Decruppe, 1997, Inhomogeneous shear flows of wormlike micelles : A master dynamic phase diagram, *Phys. Rev. E* **55**, 1668-1676.

Berret J. -F., D.C. Roux and P. Lindner, 1998, Structure and rheology of concentrated wormlike micelles at the shear-induced isotropic-to-nematic transition, *Eur. Phys. J. B* **5**, 67-77.

Bonn D., J. Meunier, O. Greffier, A. Al-Kahwaji and H. Kellay, 1998, Bistability in non-Newtonian flow : rheology and lyotropic liquid crystals, *Phys. Rev. E* **58**, 2115-2118.

Boukany P.E. and S.Q.Wang, 2008, Use particle-tracking velocimetric and flow birefringence to study nonlinear flow behavior of entangled wormlike micellar solution: From wall slip, bulk disentanglement to chain scission, *Macromolecules* **41**, 1455.

Briels W.J., D. Vlassopoulos, K. Kang and J.K.G. Dhont, 2011, in preparation.

Briels W.J., 2009, Transient forces in flowing soft matter, *Soft Matter* **5**, 4401-4411.

Britton M.M. and P.T. Callaghan, 1999, Shear banding instability in wormlike micellar solutions, *Eur. Physics J.* **B7**, 237-249.

Britton M.M., R.W. Mair, R.K. Lambert amd P.T. Callaghan, 1999, Transition to shear banding in pipe and Couette flow of wormlike micellar solutions, *J. Rheol.* **43**, 897-909.

Britton M.M. and P.T. Callaghan, 1997, Nuclear magnetic resonance visualization of anomalous flow in cone-and-plate rheometry, *J. Rheol.* **6**, 1365-1384.

Butler S. and P. Harrowell, 2002, Factors determining crystal-liquid coexistence under shear, *Nature* **415**, 1008-1011.

Cahn J.W. and J.E. Hilliard, 1958, Free energy of a nonuniform

system. I. Interfacial free energy, *J. Chem. Phys.* **28**, 258-267.
Cahn J.W. and J.E. Hilliard, 1959, Free energy of a nonuniform system. III. Nucleation in a two-component incompressible fluid, *J. Chem. Phys.* **31**, 688-699.
Callaghan P.T., 2008, Rheo NMR and shear banding, Rheol. Acta **47**, 243-255.
Callaghan P.T., A.M. Gil, 2000, Rheo-NMR of semidilute polyacrylamide in water, *Macromolecules* **33**, 4116-4124.
Cappelaere E., J. -F. Berret, J. -P. Decruppe, R. Cressely and P. Lindner, 1997, Rheology, birefringence and small-angle neutron scattering in a charged micellar system : Evidence of a shear-induced phase transition, *Pys. Rev. E* **56**, 1869-1878.
Cates M.E. and S.M. Fielding, 2006, Rheology of giant micelles, *Advances in Physics* **55**, 799-879.
Chen L.B., C.F. Zukoski, B.J. Ackerson, H.J.M. Hanley, G.C. Straty, J. Barker and C.J. Glinka, 1992, Structural changes and orientational order in a sheared colloidal suspension, *Phys. Rev. Lett.* **69**, 688-691.
Cho K.S., 2005, A geometrical interpretation of large amplitude oscillatory shear response, *J. Rheol.* **49**, 747-758.
Dhont J.K.G. and Briels W.J., 2008, Gradient and vorticity banding, *Rheol. Acta* **47**, 257-281.
Dhont J.K.G., 1999, A constitutive relation describing the shear-banding transition, *Phys. Rev. E* **60**, 4534-4544.
Dhont J.K.G. and W.J. Briels, 2003, Festschrift on the occasion of the 60th birthday of C.G. de Kruif, Viscoelasticity of suspensions of long, rigid rods, *Coll. Surf. A : Physicochem. Eng. Aspects* **213**, 131-156.
Dhont J.K.G., W.J. Briels in *Soft Matter*, 2006, Rod-Like Brownian Particles in Shear Flow, Volume 2 ; pages 147-287, eds. G. Gompper, M. Schick, Wiley-VCH.
Dhont J.K.G., 1996, Spinodal decomposition of colloids in the initial and intermediate stages, J. Chem. Phys. **105**, 5112-5125.
Dhont J.K.G., M.P. Lettinga, Z. Dogic, T.A.J. Lenstra, H. Wang, S. Rathgeber, P. Carletto, L. Willner, H. Frielinghaus and P. Lindner, 2003, Shear-banding and microstructure of colloids in shear flow, *Far. Dissc.* **123**, 157-172.
Dhont J.K.G., 1996, Spinodal decomposition of colloids in the initial and intermediate stages, *J. Chem. Phys.* **105**, 5112-5125.
Doi M. and S.F. Edwards, *The Theory of Polymer Dynamics*, 1986 ; Clarendon Press, Oxford.
Eiser E., F. Molino, G. Porte, 2000, Nonhomogeneous textures and banded flow in a soft cubic phase under shear, *Phys. Rev. E* **61**, 6759-6764.
Eiser E., F. Molino, G. Porte and X. Pithon, 2000, Flow in micellar cubic crystals, *Rheol. Acta* **39**, 201-206.
El-Kareh A.W. and L.G. Leal, 1989, Existence of solutions for all Deborah numbers for a non-Newtonian model modified to include diffusion, *J. Non-Newtonian Fluid Mech.* **33**, 257-287.
Fardin M.A., D. Lopez, J. Croso, G. Grégoire, O. Cardoso, G.H. McKinley and S. Lerouge, 2010, Elastic turbulence in shear banding wormlike micelles, *Phys. Rev. Lett.* **104**, 178303.
Fielding S.M., 2007, Complex dynamics of shear banded flows, *Soft Matter* **3**, 1262-1279.
Fielding S.M. and P.D. Olmsted, 2003, Flow phase diagrams for concentration-coupled shear banding, *Eur. Phys. J. E* **11**, 65-83.
Fielding S.M., 2007, Vorticity structuring and velocity rolls triggered by gradient shear bands, *Phys. Rev. E* **76**, 016311/1-8.
Fielding S.M. and P.D. Olmsted, 2004, Spatiotemporal oscillations and rheochaos in a simple model of shear banding, *Phys. Rev. Lett.* **92**, 084502/1-4.
Fischer E. and P.T. Callaghan, 2001, Shear banding and the isotropic-to-nematic transition in wormlike micelles, *Phys. Rev. E* **64**, 011501-1-011501-15.
Fischer P., E.K. Wheeler and G.G. Fuller, 2002, Shear-banding structure oriented in the vorticity direction observed for equimolar micellar solution, *Rheol. Acta* **41**, 35-44.
Forest M.G. and Q. Wang, 2003, Monodomain response of finite-aspect-ratio macromolecules in shear and related linear flows, *Rheol. Acta* **42**, 20-46.
Goddard J.D., 2003, Material instability in complex fluids, *Ann. Rev. Fluid Mech.* **35**, 113-133.
Goveas J.L. and P.D. Olmsted, 2001, A minimal model for vorticity and gradient banding in complex fluids, *Eur. Phys. J. E* **6**, 79-89.
Groisman A. and V. Steinberg, 1998, Mechanism of elastic instability in Couette flow of polymer solutions : experiment, *Physics of Fluids* **10**, 2451-2463.
Helgeson M.E., M.D. Reichert, Y.T. Hu and N.J. Wagner, 2009, Relating shear banding, structure, and phase behavior in wormlike micellar solutions, *Soft Matter* **5**, 3858-3869.
Herle V., P. Fischer and E.J. Windhab, 2005, Stress driven shear bands and the effect of confinement on their structures - A rheological, flow visualization and rheo-SALS study, *Langmuir* **21**, 9051-9057.
E.K. Hobbie, 2004, elastic flow instability in nanotube suspensions, *Phys. Rev. Lett.* **92**, 048302/1-4.
Hu Y.T. and A. Lips, 2005, Kinetics and mechanism of shear banding in an entangled micellar solution, *J. Rheol.* **49**, 1001-1027.
Hu H., R.G. Larson and J.J. Magda, 2002, Measurement of wall-slip-layer rheology in shear-thickening wormy micelle solutions, *J. Rheol.* **46**, 1001-1021.
Imhof A., A. van Blaaderen and J.K.G. Dhont, 1994, Shear melting of colloidal crystals of charged spheres studied with rheology and polarizing microscopy, *Langmuir* **10**, 3477-3484.
Kang K., M.P. Lettinga, Z. Dogic and J.K.G. Dhont, 2006, Vorticity banding in rodlike virus suspensions, *Phys. Rev. E* **74**, 026307/1-12.
Kang K., M.P. Lettinga and J.K.G. Dhont, 2008, Is vorticity-banding due to an elastic instability?, *Rheol. Acta*. **47**, 499-508.
Larson R.G., E.S.G. Shaqfeh and S.J. Muller, 1990, A purely elastic instability in Taylor-Couette flow, *J. Fluid Mech*. **218**, 573-600.
Lerouge S, M. Argentina and J.P. Decruppe, 2006, Interface instability in shear-banding flows, *Phys. Rev. Lett*. **96**, 088301/1-4.
Lerouge S, J. -P. Decruppe and J. -P. Berret, 2000, Correlations between rheological and optical properties of a micellar solution under shear banding flow, *Langmuir* **16**, 6464-6474.
Lettinga M.P. and S. Manneville 2009, Competition between Shear Banding and Wall Slip in Wormlike Micelles, *Phys. Rev. Lett.* **103**, 248302.
Lettinga M.P. and J.K.G. Dhont, 2004, Non-equilibrium phase

behavior of rod-like viruses under shear flow, *J. Phys.: Condens. Matter* **16**, S3929-S3939.

Liberato M.W., F. Nettesheim and N.J. Wagner, 2006, Spatially resolved small-angle neutron scattering in the 1-2 plane: A study of shear-induced phase-separating wormlike micelles, *Phys. Rev. E* **73**, 020504/1-4.

Lin-Gibson S., J.A. Pathak, E.A. Grulke, H. Wang, J. Vermant, L. Raynaud, J. Mewis, B. Ernst and G.G. Fuller, 1999, Large-scale bundle ordering in sterically stabilized latices, *J. Coll. Int. Sci.* **211**, 221-229.

Lonetti B., J. Kohlbrecher, L. Willner, J.K.G. Dhont, M.P. Lettinga, 2008, Dynamic response of block copolymer wormlike micelles to shear flow, *J. Phys.: Condens. Matter* **20**, 404207/1-11.

Lu C. -Y.D., P.D. Olmsted, R.C. Ball, 2000, Effects of non-local stress on the determination of shear banding flow, *Phys. Rev. Lett.* **84**, 642-645.

Manneville S., 2008, Recent experimental probes of shear banding, Rheol.Acta **47**, 301-318.

Manneville S., A. Colin, G. Waton and F. Schosseler, 2007, Wall slip, shear banding, and instability in the flow of a triblock copolymer micellar solution, *Phys. Rev. E* **75**, 061502-1-061502-11.

Manneville S., J.-B. Salmon and A. Colin, 2004, A spatio-temporal study of rheo-oscillations in a sheared lamellar phase using ultrasound, *Eur. Phys. J. E* **13**, 197-212.

Masselon C., J.B. Salmon and A. Colin, 2008, Non local effects in flows of wormlike micellar solutions, *Phys. Rev. Lett.* **100**, 038301/1-4.

Mather P.T., A. Romo-Uribe, C.D. Han and S.S. Kim, 1997, Rheo-optical evidence of a flow-induced isotropic-nematic transition in a thermotropic liquid-crystalline polymer, *Macromolecules* **30**, 7977-7989.

McLeish T.C.B. and Ball R.C., 1986, A molecular approach to the spurt effect in polymer melt flow, *Journal of Polymer Science* **24**, 1735-1745.

McLeish T.C.B., 1987, Stability of the interface between two dynamic phases in capillary flow in linear polymer melts, *Journal of Polymer Science* **25**, 2253-2264.

Michel E., J. Appell, F. Molino, J. Kieffer and G. Porte, 2001, Unstable flow and nonmonotonic flow curves of transient networks, *J. Rheol.* **45**, 1465-1477.

Miller E. and J.P. Rothstein, 2007, Transient evolution of shear-banding wormlike micellar solutions, *J. Non-Newtonian Fluid Mech.* **143**, 22-37.

Muller S.J., R.G. Larson and E.S.G. Shaqfeh, 1989, A purely elastic transition in Taylor-Couette flow, *Rheol. Acta* **28**, 499-503.

Olmsted P.D., 1999, Dynamics and flow-induced separation in polymeric fluids, *Current Opinion in Colloid and Interface Science* **4**, 95-100.

Olmsted P.D., 2008, Perspectives on shear banding in complex fluids, *Rheol. Acta* **47**, 283-300.

Olmsted P.D. and C. -Y.D. Lu, 1999, Phase coexistence of complex fluids in shear flow, *Faraday Discuss.* **112**, 183-194.

Olmsted P.D. and C. -Y.D. Lu, 1999, Phase separation of rigid-rod suspensions in shear flow, *Phys. Rev. E* **60**, 4397-4415.

Olmsted P.D. and C.-Y.D. Lu, 1997, Coexistence and phase separation in sheared complex fluids, *Phys. Rev. E* **56**, R55-R58.

Olmsted P.D., 1999, Two-state shear diagrams for complex fluids in shear flow, *Europhys. Lett.* **48**, 339-345.

Pakdel P. and G.H. McKinley, 1996, Elastic instability and curved streamlines, *Phys. Rev. Lett.* **77**, 2459-2462.

Palberg T. and M. Würth, 1996, Multiphase coexistence and nonlinear rheology of colloidal dispersions as observed in an optical model capillary viscosimeter, *J. Phys. I (France)* **6**, 237-244.

Preis T., R. Biehl and T. Palberg, 1998, Phase transitions in colloidal dispersions flowing through a cylindrical capillary, *Prog. Colloid Polym. Sci.* **110**, 129-133.

Pujolle-Robic C., P.D. Olmsted and L. Noirez, 2001, Transient and stationary flow behaviour of side chain liquid-crystalline polymers : evidence of a shear-induced isotropic-to-nematic phase transition, *Eutophys. Lett.* **59**, 364-369.

Radulescu O., P.D. Olmsted, J.P. Decruppe, S. Lerouge, J. -F. Berret and G. Porte, 2003, Time scales in shear banding of wormlike micelles, *Europhys. Lett.* **62**, 230-236.

Ramos L., F. Molino and G. Porte, 2000, Shear melting in lyotropic hexagonal phases, *Langmuir* **16**, 5846-5848.

Ravindranath S., S.Q. Wang, M. Olechnowicz and R. P. Quirk, 2008, Banding in simple steady shear of entangled polymer solutions, *Macromolecules* **41**, 2663.

Ripoll M., P. Holmqvist, R.G. Winkler, G. Gompper, J.K.G. Dhont and M.P. Lettinga, 2008, Attractive colloidal rods in shear flow, *Phys. Rev. Lett.* **101**, 168302.

Rofe C.J., L. de Vargas, J. Perez-Gonzelez, R.K. Lambert and P.T. Callaghan, 1996, Nuclear magnetic resonance imaging of apparent slip effects in xanthan solutions, *J. Rheol.* **40**, 1115-1128.

Salmon J. -P., A. Colin, S. Manneville, F. Molino, 2003, Velocity profiles in shear-banding wormlike micelles, *Phys. Rev. Lett.* **90**, 228303-1 - 228303-4.

Salmon J. -B., L. Becu, S. Manneville and A. Colin, 2003, Towards local rheology of emulsions under Couette flow using Dynamic Light Scattering, *Eur. Phys. J. E* **10**, 209-221.

Salmon J. -B., S. Manneville and A. Colin, 2003, Shear-banding in a lyotropic lamellar phase. Part 1 : Time-averaged velocity profiles, *Phys. Rev. E* **68**, 051503.

Salmon J. -B., S. Manneville and A. Colin, 2003, Shear-banding in a lyotropic lamellar phase. Part 2 : Temporal fluctuations, *Phys. Rev. E* **68**, 051504.

Schmitt V., C.M. Marques and F. Lequeux, 1995, Shear-induced phase separation of complex fluids: The role of flow-concentration coupling, *Phys. Rev. E* **52**, 4009-4015.

Shaqfeh E.S.G., S.J. Muller and R.G. Larson, 1992, The effects of gap width and dilute solution properties on the viscoelastic Taylor-Couette instability, *J. Fluid Mech.* **235**, 285-317.

Shaqfeh E.S.G., 1996, Purely elastic instabilities in viscometric flows, *Annu. Rev. Fluid Mech.* **28**, 129-185.

Spenley N.A., X.F. Yuan and M.E. Cates, 1996, Nonmonotonic constitutive laws and the formation of shear-banded flows, *J. Phys. II (France)* **6**, 551-571.

Spenley N.A., M.E. Cates and T.C.B. McLeish, 1993, Nonlinear rheology of wormlike micelles, *Phys. Rev. Lett.* **71**, 939-942.

Sprakel J., E. Spruijt, M.A. Cohen Stuart, N.A.M. Besseling, M.P. Lettinga and J. van der Gucht, 2008, Shear banding and rheochaos in associative polymer networks, *Soft Matter* **4**, 1696-1705.

Tapadia P., S. Ravindranath and S.-Q. Wang, 2006, Banding in entangled polymer fluids under oscillatory shearing, *Phys. Rev. Lett.* **96**, 19600/1-4.

ten Brinke A.J.W., L. Bailey, H.N.W. Lekkerkerker, G.C. Maitland, 2007, Rheology modification in mixed shape colloidal dispersions. Part I : Pure components, *Soft Matter* **3**, 1145-1162.

van den Noort A. and Briels W.J., 2007, Coarse-grained simulations of elongational viscosities, super-position rheology and shear banding in model core-shell systems, *Macromol. Theory Simul.* **16**, 742.

van den Noort A. and W.J. Briels, 2008, Brownian dynamics simulations of concentration coupled shear banding, *J. Non-Newt. Fluid Mech.* **152**, 148-155.

van den Noort A., W.K. den Otter a and W.J. Briels, 2007, Coarse graining of slow variables in dynamics simulations of soft matter, *accepted for publication in Europhys. Lett.* **80**, 28003.

van der Gucht J., M. Lemmers, W. Knoben, N.A.M. Besseling and M.P. Lettinga, 2006, Multiple shear-banding transitions in a supramolecular polymer solution, *Phys. Rev. Lett.* **97**, 108301/1-4.

Vasquez P.A., L.P. Cook and G.H. McKinley, 2007, A network scission model for wormlike micellar solutions I. Model formulation and viscometric flow predictions, *J. Non-Newtonian Fluid Mech.* **44**, 122-139.

Vermant J., 2003, Large-scale structures in sheared colloidal dispersions, *Current Opinion in Colloid and Interface Science* **6**, 489-495.

Wilhelm M., D. Maring and H. Spiess, 1998, Fourier-transform rheology, *Rheol. Acta* **37**, 399-405.

Wilkins G.M.H. and P.D. Olmsted, 2006, Vorticity banding during the lamellar-to-onion transition in a lyotropic surfactant solution in shear flow, *Eur. Phys. J. E* **21**, 133-143.

Won Y.Y., H.T. Davis and F.S. Bates, 1999, Giant wormlike rubber micelles, *Science* **283**, 960.

Yesilata B., C. Clasen and G.H. McKinley, 2006, Nonlinear shear and extensional flow dynamics of wormlike surfactant solutions, *J. Non-Newtonian Fluid Mech.* **133**, 73-90.

Yuan X. -F., 1999, Dynamics of a mechanical interface in shear-banded flow, *Europhys. Lett.* **46**, 542-548.

Note: We note that the expressions (13,15) are obtained from a Taylor expansion of the interaction contribution with respect to the orientational order parameter (as is done in Refs. (Dhont *et al.*, 2003, 2006)). A mathematically more correct way to perform the expansion, however, is to expand with respect to orthonormal irreducible polyadic products of $\hat{\mathbf{u}}$ (see, for example Ref.(Dhont, 1996)). This again leads to the expressions (13,15), except that the volume fraction is multiplied by a factor $5/4$, and gives rise to a prefactor $1/4$ instead of $1/5$ in eq.(17). This prefactor leads to the correct value for the upper spinodal concentration of $\varphi = 4d/L$ in the absence of flow, instead of the approximate value $5(d/l)$ that is found from eq.(15).